Response to Reviewers

Referee #1

This paper shows that, within the suite of measurements they present, the nighttime formation of SA is consistent with a simplified chemistry driven by alkene, ozone, and SO_2. Yet correlation does not constitute proof. Furthermore, the procedures and details of the methodology (which may be correct) are either only sketched-out or are hard to follow (thus this reader did not have full confidence in the material.) Furthermore, the authors supply caveats (more than one time and even in the abstract!) that their analysis could be subject to revision/flawed. Providing a detailed, time-dependent simulation (even a box model) would bring their conclusion into the firmly believable realm. Below are some details and other points. Note the revisions are too strongly suggested as 'major': they are by no means damning and they should not be difficult to include or address.

We thank the reviewer for the constructive comments and suggestions. As suggested, we have added more details of the methodology to make our analysis easier to follow. We did not quite follow the comment on "the authors supply caveats (more than one time and even in the abstract!) that their analysis could be subject to revision/flawed", but we hope our point-to-point response to the comments as given below can address these concerns. The comments, our replies, and the corresponding changes in the manuscript and supplementary information are marked in black, blue, and green, respectively.

1) Somewhat careless with precision, quoting a four significant figure k_{app} from a slope that has at most two significant figures. A minor detail of course, but attention to detail should be demonstrated in all aspects. A welcome detail here would be to present the uncertainties in the values of the fitted slopes.

Response: Thanks a lot for your suggestions and we have revised the k_{app} values with two significant figures.

The fitted value, 95% confidence bounds, uncertainty of k_{app} and correlation coefficient R^2 for Clean-1 (Fig. 5(a)) and Clean-2 (Fig. 5(b)) condition are listed in Table S3. The uncertainties of k_{app} are 20.2% and 11.3% for Clean-1 and Clean-2 condition respectively.

For nighttime correlation between source term and sink term in Section 4.3 and Fig. 5, we mentioned in the manuscript that only under Clean-2 condition, there was a good correlation (R^2=0.97) for the mean values in all bins (Fig. 5 (b), Line 229-231, Page 9). For Clean-1 condition, there was only a subgroup of binned data with a source range from 1.0×10^{33} to 4.5×10^{33} $(cm^{-3})^3$ that showed linear correlation (Line 223-224, Page 9). And for heavy polluted condition, no correlation was observed. (Line 253-254, Page 10).

We have also added one sentence in the manuscript to refer to this table. "The fitted value, 95% confidence bounds, uncertainty of k_{app} and correlation coefficient R^2 for Clean-1 and Clean-2 condition are listed in Table S3." (Line 233-234, Page 9).

Table S3 Fitted value, 95% confidence bounds, uncertainty of k_{app} and R^2 for Clean-1 and Clean-2 condition.

Condition	k_{app} (cm^6 s^{-1})	95% Confidence Bounds (cm^6 s^{-1})	Uncertainty (%)	R^2
Clean-1	2.7×10^{-30}	(2.1×10^{-30} - 3.2×10^{-30})	20.2	0.97
Clean-2	2.6×10^{-30}	(2.3×10^{-30} - 2.9×10^{-30})	11.3	0.97

2) Overall sink was equated to the alkene O_3 SO_2 source but steady-state assumption was not fully discussed (not even sure what time period the data is averaged over?).

Response: The verification of the steady-state assumption is indeed necessary. We have added the following content in Section S2 to clarify why steady-state assumption can be assumed.

The net concentration change of gaseous SA is determined by both the source and loss terms, as shown in the following equation:

$$\frac{d[SA]}{dt} = k_{app} \cdot [Alkene] \cdot [O_3] \cdot [SO_2] - [SA] \cdot CS - \beta \cdot [SA]^2$$

We can compare the magnitude of the net concentration change to the overall loss rate. During nighttime (20:00-04:00) from 18th January to 16th March 2019, the median net concentration change of SA is about 181.60 $cm^{-3}s^{-1}$ and the overall SA loss rate at the median SA concentration (7.52×10^5 cm^{-3}) is 1.61×10^4 $cm^{-3}s^{-1}$. As the loss rate (and source rate) is much faster than the net concentration change, the pseudo-steady state (PSS) assumption is valid for SA. Besides, the resolution of the SA data is 5 minutes, and the concentration, net concentration change, loss rate and production rate of SA are listed in Table S4 below.

Table S4 Concentration, net concentration change, loss rate and production rate of SA during nighttime (20:00-04:00) from 18th January to 16th March 2019. Std means standard deviation.

	[SA] (cm^{-3})	d[SA]/dt ($cm^{-3}s^{-1}$)	L_{SA} ($cm^{-3}s^{-1}$)	P_{SA} ($cm^{-3}s^{-1}$)
Median	7.52×10^5	181.60	1.61×10^4	1.60×10^4
25 percentile	5.19×10^5	78.37	4.83×10^3	4.80×10^3
75 percentile	1.05×10^6	371.14	3.27×10^4	3.26×10^4

To clarify this consideration, we added the above explanation in the revised supplement as Section S2 (Line 16-25, Page 1) and the following sentence in the revised manuscript:

"Under pseudo steady-state (PSS) assumption (see Section S2 for detailed disscussion about PSS assumption)" (Line 216-217, Page 8)

The time periods of the data in Fig. 5 and Fig. 6 are both from 18th January to 16th March 2019. Corresponding illustrations were added to the captions of Fig. 5 (Line 249, Page 10) and Fig. 6 (Line 285, Page 11).

3) Furthermore, SO_3 to SA was not discussed.

Response: Indeed, we did not discuss the conversion from SO_3 to SA, as the reaction is so fast that almost all SO_3 should be instantaneously converted to SA. To be more specific, the conversion of SO_3 to SA is based on the following reaction:

$$SO_3 + 2H_2O \xrightarrow{k} H_2SO_4 + H_2O$$

Then, the production rate of SA from SO_3 can be expressed as:

$$P_{[SA]} = k \cdot [SO_3] \cdot [H_2O]^2$$

where $k=3.9\times10^{-41}\exp(6830.6/T)\ cm^{-6}\ s^{-1}$ ((Jayne et al., 1997)). During the nights of the measurement period, the median concentration of H_2O was $4.97\times10^{16}\ cm^3$, and the median temperature was 276.6 K, then the lifetime of SO_3 can be estimated as:

$$\tau_{SO_3} = \frac{1}{k \cdot [H_2O]^2} = \frac{1}{4.88\times10^3\ s^{-1}} = 2.05\times10^{-4}\ s$$

As the lifetime of SO_3 is so short under typical atmospheric conditions, the oxidation of SO_2 is the rate-limiting step in the formation of SA.

To clarify this consideration, we added the above illustration in Section S1 (Line 2-14, Page 1) and the following explanation in the revised manuscript:

"The lifetime of SO_3 due to its fast reaction with H_2O to form SA is approximately 2×10^{-4} s (see detailed calculation in supplement Section S1), which indicates that this reaction is so fast that almost all SO_3 will be instantaneously converted to SA. In this case, the oxidation of SO_2 is the rate-limiting step in the formation of SA." (Line 84-86, Page 3)

4) OH produced in alkene + O_3 reactions was not included: why not?

Response: This is a misunderstanding. We didn't mean to exclude the non-photochemical ·OH oxidation pathway. Actually, we do not attempt to separate the contributions of sCI and OH radical in this study, but instead, use the k_{app} as an empirical parameter to account for the overall effect of sCI and OH oxidation pathways.

We realized that the comparison between k_{app} and theoretical sCI oxidation rate is confusing that caused the misunderstanding. Besides, such comparison also suffers from large uncertainties. Therefore, we decide to remove such discussion in the revised manuscript so that the main message can be clearer. However, we need to point out that, this change in the manuscript will not change our conclusion that the ozonolysis of alkenes is responsible for the oxidation reactions (both sCI and non-photochemical OH radical) that drive the nighttime SA formation.

To clarify this consideration, the following illustration are added to the revised manuscript:

"The ozonolysis of alkenes under dark conditions is capable of generating sCI as well as OH radical, both of which are able to oxidize SO_2 to form gaseous SA. However, the yields of both sCI and recycled OH radical remain largely unquantified. Therefore, we do not attempt to distinguish the contribution of sCI and OH radical on SA formation in this study, but rather treat them as a "bulk oxidant" and use an empirical parameter k_{app} to account for both oxidation pathways." (Line 205-209, Page 8)

And the following discussion are deleted from the revised manuscript:

"In order to have a general understanding of the apparent rate constant of sCI-SO_2 reaction obtained from our measurement, we can roughly get an upper limit value by considering all nighttime SA is produced from the sCI mechanism. From the above discussion, the slope k_{app} can be expressed as $k_1 \cdot k_2 \cdot \varphi \cdot f$, where f is the fraction of sCI which undergo the reaction with SO_2. It should be pointed out that k_2 is also an apparent rate constant which results from the combination of different measurement efficiency of alkenes (including undetected ones), different yields of sCI, and different rate constants of sCI reacting with SO_2. The fitted k_{app} is $2.618\times10^{-30}\ cm^6\ s^{-2}$. If considering k_1 to be $1.0\times10^{-17}\ cm^3s^{-1}$ (an intermediate value in the range of previous studies, which has been explained in Section 2), then $k_2 \cdot \varphi \cdot f = 2.618\times10^{-13}\ cm^3s^{-1}$. As the real atmospheric chemical composition is far more complex than experimental ones, the value of φ·f should be smaller. Thus, if further considering φ·f to be 0.05, then the rate constant k_2 in this real atmospheric condition is approximate $5.236\times10^{-12}\ cm^3s^{-1}$, which is in the same order of magnitude as measured values in experiments (see Section 2)." (between Line 234 and Line 235, Page 9)

5) A simple box model could include these and others such as HO_2 + NO for example. Then presenting box model simulations absent the alkene-ozone chemistry might really draw a distinct comparison.

Response: Performing a well-tuned box model is indeed a useful way of verifying our findings. However, after thinking it through, we found that many species and parameters needed for the box model remain unquantified or largely uncertain. For example, the concentration of OH radical in the nighttime is one key parameter in such a box model, but lacking of a complete VOC measurement by GCMS will greatly limit the precision of the box model. And recent study also showed that current MCM method significantly under-predicts the concentrations of OH, HO_2 and RO_2 radicals. (Slater et al., 2020) Besides, the yields of sCI and OH radical as well as the rate constants concerning R1 to R5 of alkenes are largely scattered (Line 90-94 Page 3). Therefore, we prefer not to include the box model simulation in this manuscript, but clearly state the need for a box model based on further lab studies to fully to verify our results.

To clarify this consideration, the following discussion has been added to the revised manuscript:

"It should be pointed out that we are not able to further deconvolute the contribution of OH radical and sCI based on the ambient observation. A well-tuned box model is a useful tool to resolve it and verify the role of the ozonolysis of alkenes on the nighttime SA formation. However, such a modeling work is not included in our study, as the lacking of a complete VOC datasets in our measurement and the largely uncertain yields of sCI from the ozonolysis of various alkenes have caused challenges in ensuring the precision of the box-model." (Line 263-267, Page 10)

6) Is not sub-3 nm really sub-2.45 nm?

Response: Such a particle size range is determined by the instrument (PSM). According to the calibration of the instrument, the size bins of PSM are 1.3-1.44 nm, 1.44-1.5 nm, 1.5-1.61 nm, 1.61-1.81 nm and 1.81-2.45 nm, and the number concentration of sub-3nm particles is the sum of all those five size bins. Uncertainties in response of PSM to particles of different chemical composition (Kangasluoma et al., 2014) can shift the overall size-range where the PSM is sensitive, which is the reason why the total concentration measured between the lowest and highest size in PSM is generally referred as sub-3 nm particle concentration (see e.g. (Kontkanen et al., 2017)).

To clarify this consideration, the following sentence has been added to the revised manuscript:

"(…) was measured with a Particle Sizer Magnifier (PSM) (Vanhanen et al., 2011), and the integrated number concentration of particles from PSM is referred as $N_{Sub\text{-}3nm}$ in the following" (Line 139-140, Page 5)

7) The last figure purports to correlate sub-3 nm to measured SA and there is a linear relationship provided. Two problems: large error bars (what do they mean?) and there is a source of particles at zero SA (or zero alkene+ozone). The correlation may be due to the fact that the ordinate and abscissa are both dependent on the alkene-O_3 chemistry yet sub-3 nm particles at 'zero' chemistry destroys the happiness of the association between ordinate and abscissa. Another issue is the lack of discussion regarding any proposed theoretical relationship between SA and number of particles.

Response: The large error bars indicate the scattering of those data points in each bin. For better illustration, we revised this plot with boxplots in SA bins (see below), which provide direct information on the data distribution. In the boxplot, the red line is the median value, the bottom and top blue lines are the 25 and 75 percentiles, and the whisker ranges cover the ± 2.7σ of those data in each bin. In addition, the mean values are added as diamonds.

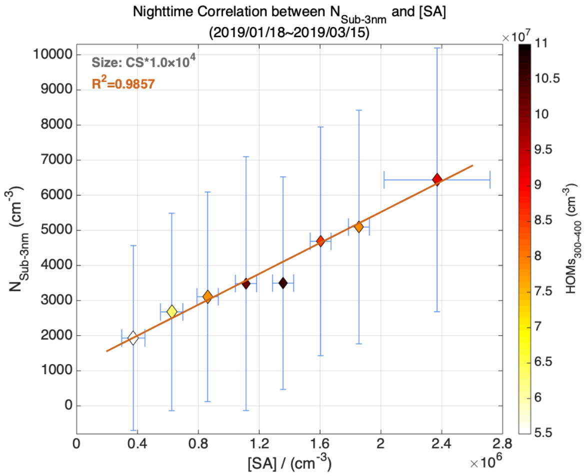

Original Fig. 5 Nighttime correlation between $N_{Sub\text{-}3nm}$ and SA concentration during nighttime (20:00-04:00) from 18th January to 16th March 2019. The data points are colored by number concentration of HOM (m/Q = 300 - 400 Th) and the size is related to CS. Note that the data points are based on the binned data instead of the original one.

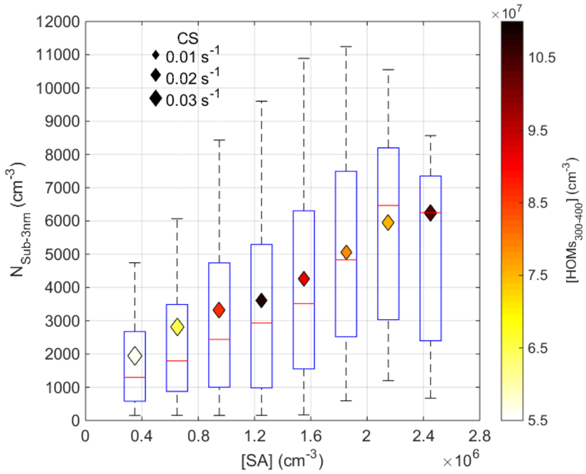

Updated Fig. 5 Correlation between $N_{Sub\text{-}3nm}$ and SA during nighttime (20:00-04:00) from 18th January to 16th March 2019. The binned diamonds are colored by number concentration of HOMs (m/Q = 300 - 400 Th) and the size is related to CS. The red line is the median value, the bottom and the top blue lines are the 25 and 75 percentiles, and the whisker ranges cover the ± 2.7σ of those data in each bin.

To clarify this consideration, we replaced the original Fig. 5 with the updated one in the manuscript. Please also note that Fig. 5 becomes Fig. 6 in the revised manuscript.

The particles at zero SA were most likely from other sources than SA. As we mentioned, our measurement site is close to two main urban traffic trunk roads, and these particles might come from directly emission of vehicles (Arnold et al., 2006;Barrios et al., 2012). In a recent study, it is shown that PSM is very sensitive to traffic-emitted sub-3nm particles (Ronkko et al., 2017).

Regarding the theoretical relationship between number concentration of sub-3nm particles and SA concentration, it is usually done by depicting the particle nucleation rate (J, e.g., $J_{1.5}$, $J_{1.7}$) as a function of SA concentration, and comparing it with other chamber or ambient studies with known mechanisms. Calculation from number concentration (N) to J involves many corrections including the correction of particle growth out of the size range. However, in these nighttime SA events, the determination of particle growth rate is challenging as the “banana shape” is not clear (please also see the reply to comment #2) of the other reviewer). This is the main reason why we used the number concentration, as a more objective term, instead of the calculated particle nucleation rate in this study.

However, to address the reviewer’s concern, we estimated J by ignoring the growth rate correction term in the calculation. Fig. R1 shows the correlation between $J_{1.5}$/$J_{1.7}$ and SA for Beijing measurement, Shanghai measurement (Almeida et al., 2013) and CLOUD experiments (Almeida et al., 2013;Kirkby et al., 2011). As shown in Fig. R1, data points in the nighttime and the daytime are roughly falling on the same line, which also agree well with the data measured in Shanghai CLOUD chamber SA-DMA-H_2O experiment. The similar J – SA relationship between the nighttime and the daytime suggests a similar nucleation mechanism as SA-base clustering. However, as the calculation of J has the aforementioned uncertainty, we prefer not to include Fig. R1 in the manuscript.

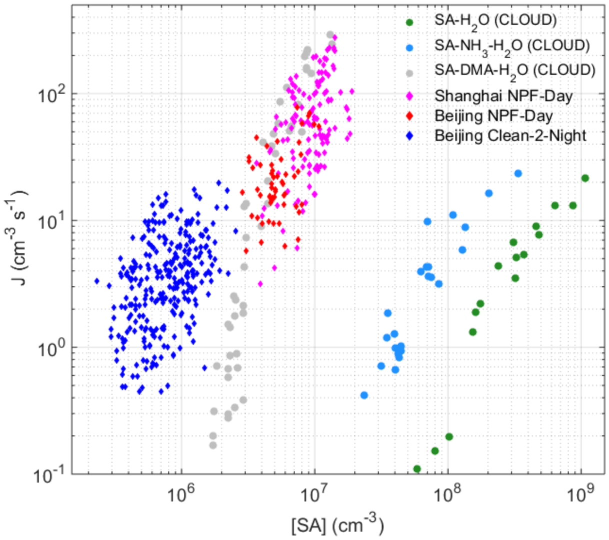

Fig. R1 Comparison of Beijing ambient, Shanghai ambient and CLOUD experimental cluster formation rates against SA concentration. Green, light blue and grey dots denote CLOUD $J_{1.7}$ data for SA-H_2O, SA-NH_3- H_2O and SA-DMA- H_2O nucleation respectively (Almeida et al., 2013;Kirkby et al., 2011). Magenta diamonds represent Shanghai NPF $J_{1.7}$ data (Yao et al., 2018). Red and blue diamonds are Beijing $J_{1.5}$ data for NPF day (10:00-14:00) and Clean-2 night (20:00-04:00), respectively.

Furthermore, there was a negative correlation between $N_{Sub-3nm}$ and highly oxygenated organic molecules (HOMs) (see Fig. S8 (a) below), which indicates that HOMs was not the main driver for the formation of nighttime sub-3nm particles. And to clarify this consideration, we added Fig. S8 (a) in the revised supplement.

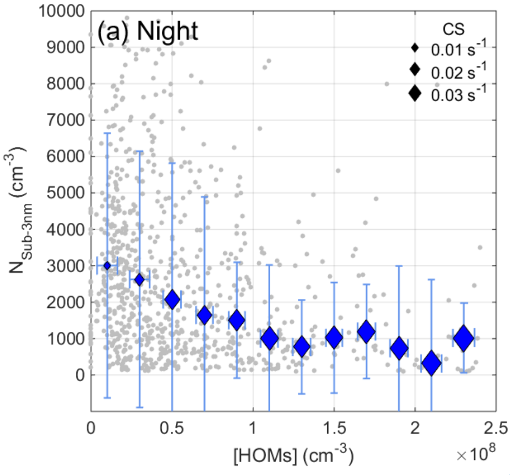

Fig. S8 (a) Correlation between $N_{Sub-3nm}$ and [HOMs] during nighttime (20:00-04:00) from 18th January to 16th March 2019. The grey dots are original data points. The diamonds are binned data colored by number concentration of SA and the size is proportional to CS. The blue lines are standard deviation of data points in each bin.

8) The outliers are numerous in many of the plots in Fig. 2. How were they decided upon? In this vein it is not clear what data was included for each of the points in Fig. 4 for example. All data between 10 pm and 4 am?

Response: Please note that now Fig. 2 is Fig. 3, and Fig. 4 is Fig. 5.

The outliers in Fig. 3 are the ones out of the ± 2.7σ range of all selected data. If the data is normally distributed, this ± 2.7σ range will cover 0.7 - 99.3 percentiles of the data. Corresponding illustrations have been added to the captions of Fig. 3 (Line 186, Page 7) in the revised manuscript.

Data points in Fig. 5 are the ones during nighttime (20:00-04:00) from 18th January to 16th March 2019. Corresponding illustrations have been added to the captions of Fig. 5 (Line 249, Page 10). Fig. 5 (a), (b), (c) and (d) are for Clean-1, Clean-2, mildly polluted and heavy polluted conditions respectively. The definition of Clean-1, Clean-2, mildly polluted and heavy polluted conditions have been illustrated in the manuscript (Line 199-201, Page8 and Line 226-227, Page 9). For better understanding of Fig. 5, the legends in four subplots have been changed from 'Vis ≥ 12 km', 'Vis ≥ 16 km, $[O_3] \geq 2\times10^{11}$ cm^{-3}', 'Vis: 4-12 km' and 'Vis ≤ 4 km' to 'Clean-1', 'Clean-2', 'Mildly polluted' and 'Heavy polluted' accordingly.

9) "SIZE = CS*xyz" was included in many of the plots but a reference size was not easy to find.

Response: Thanks a lot for your suggestions. We've added three CS references points (CS=0.01 s^{-1}, 0.02 s^{-1} and 0.03 s^{-1}) in all relevant plots.

10) " calibration coefficient " has no meaning by itself. Needs some context (an equation) and perhaps some comparisons. It can be argued that this quantity should have units of Hz Hz-1 attached to it also.

Response: Thanks for your suggestion. We have now added the following equation to clarify how SA concentration is calculated.

The quantification of sulfuric acid is derived from the ratio of bisulfate ions relative to primary ions as follows:

$$[H_2SO_4] = \frac{HSO_4^- + H_2SO_4NO_3^-}{NO_3^- + HNO_3NO_3^- + (HNO_3)_2NO_3^-} \times C$$

The calibration factor, C, is determined from direct calibration where gaseous sulfuric acid of known amounts is produced and injected into the instrument. A more detailed information about the calibration is discussed by Kürten et al. 2012 (Kurten et al., 2012) . The units of bisulfate and primary ions are both counting rates in ions·s^{-1} and cancel each other, and therefore, the unit of C is the same as that of sulfuric acid concentration in cm^{-3}.

To clarify this consideration, we added the following illustration in the revised manuscript:

"The quantification of sulfuric acid is derived from the ratio of bisulfate ions (with counting rates unit in ions·s^{-1}) relative to primary ions as follows:

$$[H_2SO_4] = \frac{HSO_4^- + H_2SO_4NO_3^-}{NO_3^- + HNO_3NO_3^- + (HNO_3)_2NO_3^-} \times C$$

The calibration factor, C, is determined from direct calibration by injecting gaseous sulfuric acid of known amounts into the instrument (Kurten et al., 2012)." (Line 114-118, Page 4)

11) Why have PM2.5, visibility and CS all plotted in Fig. 2? Figure 2 would be cleaner if you pick one and plot the correlation between it and the others in the supplement....

Response: Thanks for your suggestion and please note that Fig. 2 now is Fig. 3. The correlation among these three parameters have been shown in Fig. S3.

From the perspective of cleanliness, picking one parameter among $PM_{2.5}$, visibility and CS, and moving the correlation figure to the supplement is reasonable. $PM_{2.5}$ is the most commonly used parameter to describe pollution level, visibility is used to distinguish pollution level in Section 4.3, and nighttime SA events were highly associated with CS level (Table S2). As all these parameters are useful for the later discussion, we are prone to keep them in the current form.

Referee #2

This paper presents gas phase sulfuric acid measurements from Beijing during winter and summer with CIMS and show some nighttime formation of sulfuric acid, possibly from sCI formed from VOCs ozonolysis reactions. Sulfuric acid measurements are valuable – considering roles of sulfuric acid on new particle formation especially in urban environments. But data analysis is not effective – please see comments below. The other conclusion is nighttime sulfuric acid is responsible for sub-3 nm particles. How did the authors exclude HOMs from sub-3 nm particle formation?

We thank the reviewer for the constructive comments and suggestions and we have carefully revised our manuscript and supplement accordingly. The point-to-point response to the comments is given below. The comments, our replies, and the corresponding changes in the manuscript and supplementary information are in black, blue, and green, respectively. In this study, HOMs are not likely the determining species for the formation of sub-3nm particles and detailed discussions are shown in the response to question '3)'.

1) Section 4.3. I have never seen a kinetic expression like this: $k_{app} \cdot [Alkene] \cdot [O_3] \cdot [SO_2]$. This does not make sense to me. Please show how k_{app} is the same as $k_1 \cdot k_2 \cdot \varphi \cdot f$? And what about k_3, k_4 and k_5 then? Does this mean nighttime sulfuric acid is not from OH + SO_2 reaction (OH from VOCs ozonolysis)? The authors assume are really from sulfuric acid clusters?

Response: Both sCI and non-photochemical ·OH are capable of oxidizing SO_2 to form SA at night. Actually, the contribution of sCI and OH radical cannot be distinguished in our study, and k_{app} expressed by $k_1 \cdot k_2 \cdot \varphi \cdot f$ in the original manuscript was used to roughly get an upper limit of the sCI oxidation pathway by assuming the contribution of OH radical is negligible. But we found this part of discussion caused much confusion and decided to remove it from the revised manuscript.

The $k_{app} \cdot [Alkene] \cdot [O_3] \cdot [SO_2]$ is an informal expression of describing the formation rate of SA, where k_{app} is an overall empirical parameter that takes into account the OH radical and sCI oxidation pathways resulted from the ozonolysis of alkenes. We use this empirical parameter because the detailed chemical formation pathways and corresponding parameters from alkenes, O_3 and SO_2 to SA are still not fully quantified yet.

To clarify this consideration, the following illustration are added to the revised manuscript:

"The ozonolysis of alkenes under dark conditions is capable of generating sCI as well as OH radical, both of which are able to oxidize SO_2 to form gaseous SA. However, the yields of both sCI and recycled OH radical remain largely unquantified. Therefore, we do not attempt to distinguish the contribution of sCI and OH radical on SA formation in this study, but rather treat them as a "bulk oxidant" and use an empirical parameter k_{app} to account for both oxidation pathways." (Line 205-209, Page 8)

And the following discussion are deleted from the revised manuscript:

"In order to have a general understanding of the apparent rate constant of sCI-SO_2 reaction obtained from our measurement, we can roughly get an upper limit value by considering all nighttime SA is produced from the sCI mechanism. From the above discussion, the slope k_{app} can be expressed as $k_1 \cdot k_2 \cdot \varphi \cdot f$, where f is the fraction of sCI which undergo the reaction with SO_2. It should be pointed out that k_2 is also an apparent rate constant which results from the combination of different measurement efficiency of alkenes (including undetected ones), different yields of sCI, and different rate constants of sCI reacting with SO_2. The fitted k_{app} is 2.618×10^{-30} cm^6 s^{-2}. If considering k_1 to be 1.0×10^{-17} cm^3s^{-1} (an intermediate value in the range of previous studies, which has been explained in Section 2), then $k_2 \cdot \varphi \cdot f = 2.618\times10^{-13}$ cm^3s^{-1}. As the real atmospheric chemical composition is far more complex than experimental ones, the value of $\varphi \cdot f$ should be smaller. Thus, if further considering $\varphi \cdot f$ to be 0.05, then the rate constant k_2 in this real atmospheric condition is approximate 5.236×10^{-12} cm^3s^{-1}, which is in the same order of magnitude as measured values in experiments (see Section 2)." (between Line 234 and Line 235, Page 9)

The reviewer also asked that "The authors assume are really from sulfuric acid clusters?". Does the reviewer mean to ask that "Is the nighttime sub-3nm particles are formed from SA clusters?". And our answer is yes. As shown in Fig. 6 (please note that original Fig. 5 now is Fig. 6), there was a positive linear correlation between $N_{sub\text{-}3nm}$ and SA, suggesting that SA was the main driving species for sub-3nm particles formation. Detailed discussion on the formation mechanism of sub-3nm particles is shown in response to comment '3)' and '4)'.

2) Please also include size distributions to show if there are new particle formation or not during the night.

Response: As particles measured by PSM only cover the size range of 1.3 nm to 2.45 nm, which is not able to show whether there is new particle formation or not, we plotted the size distribution of negative ions measured by neutral cluster and air ion spectrometer (NAIS) (Fig. R2). In general, among 57 nights from 18th January to 15th March 2019, there were 9 nights with elevated sub-3nm ions (marked with black rectangles in Fig, R2), but further growth of sub-3nm clusters was not observed.

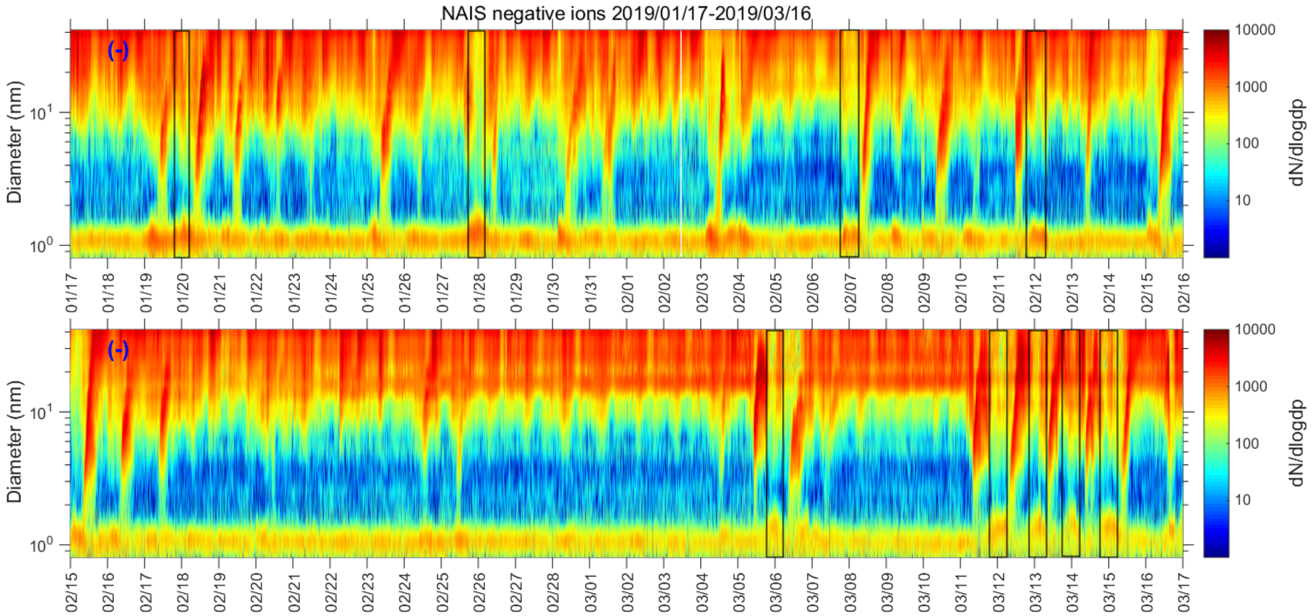

Fig. R2 Size distribution of negative ions (measured by NAIS) from 17th January to 16th March 2019. Nights with elevated sub-3nm negative ions are marked with black rectangles. The size distribution of positive ions is similar to that of negative ions and therefore are not shown here.

3) Figure 5. Please also show HOMs in the same way as sulfuric acid, and include day-time data as well (vs. nighttime). Did sub-3 nm particles grow further? If they did not grow larger, then what are the possible explanations?

Response: The correlation between $N_{\mathrm{Sub\text{-}3nm}}$ and concentration of HOMs for both day and night are shown below (and have been added to supplement as Fig. S8).

There was a negative relationship between $N_{\mathrm{Sub\text{-}3nm}}$ and HOMs for both nighttime and daytime, indicating that HOMs were not the main driver for the formation of sub-3nm particles. This phenomenon is in contrast with some previous observations in forested areas where oxidation products of biogenic VOCs, especially monoterpene, were the main contributor to the formation of clusters (Eerdekens et al., 2009;Lehtipalo et al., 2011;Kammer et al., 2018;Rose et al., 2018). Both observation (Rose et al., 2018) and laboratory experiment (Lehtipalo et al., 2018) have shown that HOMs dimers with extremely low volatility play a key role in the initial formation of clusters, while at our site, the high level of NO_x inhibited the production of HOM dimers and almost all HOMs are monomers, which are of minor importance to the formation of sub-3nm particles.

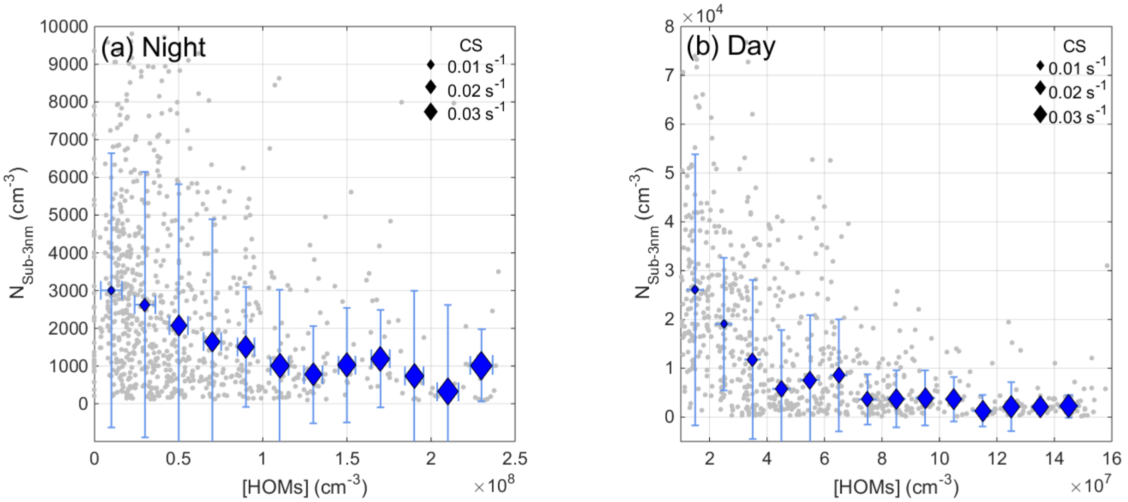

Fig. S8 Correlation between $N_{\mathrm{Sub\text{-}3nm}}$ and [HOMs] for (a) during nighttime (20:00-04:00) and (b) during daytime (09:00-16:00) from 18th January to 16th March 2019. Grey dots are original data, and diamonds are binned ones colored by SA concentration. The size of the binned data is proportional to CS and blue lines are standard deviation of each binned data.

To clarify this consideration, we added Fig. S8 in the revised supplement and the following interpretation in the revised manuscript:

"Different from SA, there was a negative correlation between the concentration of highly oxygenated organic molecules (HOMs) and $N_{\text{Sub-3nm}}$ for both nighttime and daytime (see Fig. S8 in the supplement), indicating that HOMs were not the main driver for the formation of sub-3nm particles. This phenomenon is in contrast with some previous observations in forested areas where oxidation products of biogenic VOCs, especially monoterpene, were the main contributor to the formation of clusters (Eerdekens et al., 2009;Lehtipalo et al., 2011;Kammer et al., 2018;Rose et al., 2018). Both observation (Rose et al., 2018) and laboratory experiment (Lehtipalo et al., 2018) have shown that HOM dimers with extremely low volatility play a key role in the initial formation of clusters; however at our site in urban Beijing, high level of NO_x inhibited the production of HOM dimers and most HOMs are monomers, which have minor importance to the formation of sub-3nm particles." (Line 272-281, Page 11)

As also shown in Fig. R2, these newly formed particles during the nighttime events are not able to grow to larger sizes. A similar phenomenon was also observed in a Finnish boreal forest (Rose et al., 2018). The reason remains unclear. But the hypothesis is that there is lacking of photochemistry and enough production of essential vapors that dominate the particle growth.

4) Can you calculate J from PSM? What is p (power dependence) of J or sub-3 nm particles on nighttime sulfuric acid (vs. daytime)? Is p different during day and night?

Response: Calculating particle nucleation rate (J) from number concentration (N) involves many corrections including the correction of particle growth out of the size range. However, in these nighttime SA events, the determination of particle growth rate is challenging as the "banana shape" is not clear (please also see the reply to comment #2). This is the main reason why we used the number concentration, as a more objective term, instead of the calculated particle nucleation rate in this study.

However, in order to address the reviewer's concern on the power dependence, we calculated J by ignoring the particle growth correction. The J as a function of SA concentration is plotted in Fig. R1, including the data in our measurement as well as the reported ones in Shanghai measurement (Yao et al., 2018) and the CLOUD chamber experiments (Almeida et al., 2013;Kirkby et al., 2011) as references. As shown in Fig. R1, data points in the nighttime and the daytime are roughly falling on the same line, which also agree well with the data measured in Shanghai and CLOUD chamber SA-DMA-H_2O experiment. The similar J – SA relationship between the nighttime and the daytime suggests a similar nucleation mechanism as SA-base clustering.

The p value (fitted using $J=k*[SA]^p$) of nighttime data alone, daytime data alone, Shanghai data alone, as well as all those three data set together are 0.64, 1.3, 0.87, and 1.1, respectively. However, it should be noted that, the p value may also differ significantly due to different cluster loss rate even when the nucleation mechanism is the same and may also be influenced by the more scattered data in the ambient measurement. This can be seen when comparing the p value of SA-DMA-H_2O data in the CLOUD experiment ($p = 2.4$) and the data in Shanghai ($p = 0.87$). Therefore, a detailed discussion on p values was not included in this study. In addition, as the calculation of J has the aforementioned uncertainty, we did not include the Fig. R1 in the manuscript.

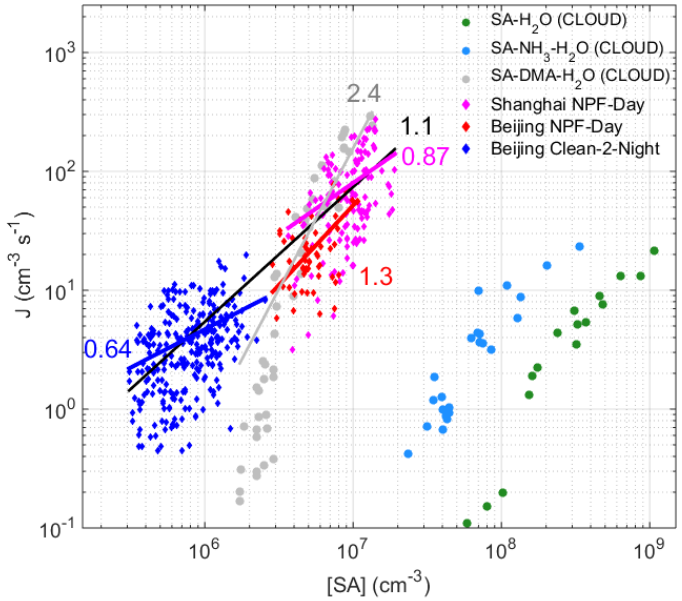

Fig. R1 Comparison of Beijing ambient, Shanghai ambient and CLOUD experimental cluster formation rates against SA concentration. Green, light blue and grey dots denote CLOUD $J_{1.7}$ data for SA-H_2O, SA-NH_3- H_2O and SA-DMA- H_2O nucleation respectively (Almeida et al., 2013;Kirkby et al., 2011). Magenta diamonds represent Shanghai NPF $J_{1.7}$ data (Yao et al., 2018). Red and blue diamonds are Beijing $J_{1.5}$ data for NPF day (10:00-14:00) and Clean-2 night (20:00-04:00), respectively. The red, blue, magenta and black lines are linear fits for Beijing NPF days, Beijing Clean-2 nights, Shanghai NPF days as well as all those three data set together respectively. The grey line is the linear fit for CLOUD SA-DMA- H_2O experiments.

5) Line 40: Needs refs., e.g., [Lee et al., 2019].
Line 43: Please include [Yu et al., 2012].
Line 51: please include [Erupe et al., 2010] and [Yu et al., 2013]

Response: Thanks a lot for your suggestions and we have added these references (Line 40, 43 and 51, Page 2).

6) Line 54: needs refs. Is this statement true? I hardly see e7 cmˆ-3 level of sulfuric acid.

Response: Many urban and rural agricultural lands that are dominantly influenced by human activities had daily maximum concentration of SA that was around or exceeded 1×10^7 cm^{-3} during summer. Reported places include Hohenpeissenberg in Germany (Birmili et al., 2003), Heidelberg in Germany (Fiedler et al., 2005), Atlanta of Georgia in the US (McMurry et al., 2005), Tecamac in Mexico (Iida et al., 2008), Kent of Ohio in the US (Erupe et al., 2010), Melpitz in Germany (Paasonen et al., 2010), San Pietro Capofiume in Italy (Paasonen et al., 2010), Beijing in China (Wang et al., 2011), village of Viebrunn in Germany (Kuerten et al., 2016) and Shanghai in China (Yao et al., 2018). And these references have been added in the revised manuscript (Line 55-56, Page 2).

Besides, the daily maximum concentration of SA at our site during 2019 summer also frequently exceeded 1×10^7 cm^{-3} (Fig. R3), which may result from high level of SO_2 (see detailed explanation in response to question '11)') and OH radical.

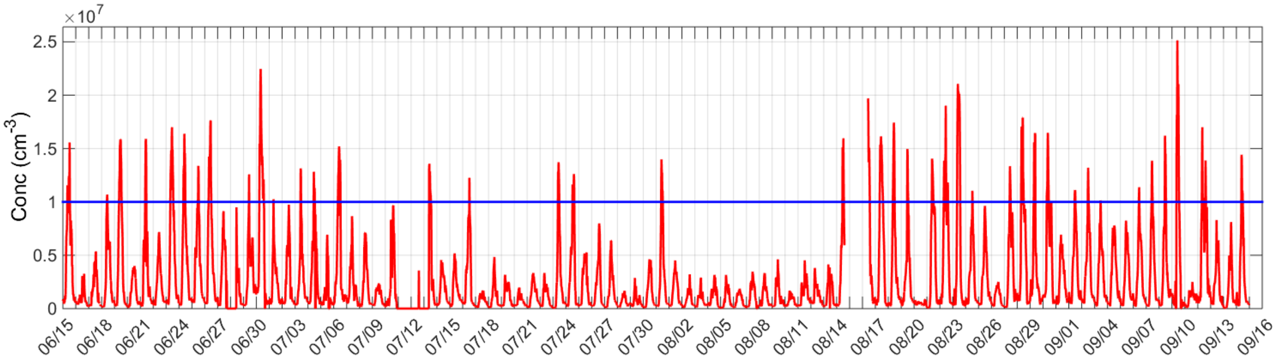

Fig. R3 Time variation of SA concentration from 15th June to 14th September 2019. The concentration of 1×10^{7} cm^{-3} is marked by blue line.

7) Line 60: please include [Yu et al., 2013].

Response: Thanks a lot for your suggestion and we have added this reference (Line 63, Page 2).

8) Line 64: Change "frequent and noticeable" to "noticeable nighttime sulfuric acid sometimes".

Response: Thanks a lot for your suggestion and we have changed "frequent and noticeable" to "noticeable nighttime sulfuric acid sometimes" as suggested (Line 66-67, Page 3).

9) Line 105: This is a very long inlet. What is the residence time, and radius? Wall loss rate in the inlet?

Response: The length and radius of the inlet of nitrate-LToF-CIMS is 1.6 m and of 3/8 inch respectively. Based on the 7.2 L min^{-1} sample flow rate, the residence time is:

$$\mathrm{t}=\frac{(\pi\cdot R^{2})\times L}{Q}=\frac{3.14\times(9.525\times10^{-3}\ m)^{2}\times(1.6\ m)}{7.2\times10^{-3}\ m^{3}\ min^{-1}}\approx 0.0633\ min\approx 3.80\ s$$

The SA transport efficiency with diffusional wall loss in the inlet, $\eta_{SA,\ inlet}$, is calculated according to the Gormley and Kennedy equation (Kulkarni et al., 2011):

$$\eta_{SA,inlet}=\begin{cases}1-2.56\xi^{\frac{2}{3}}+1.2\xi+0.177\xi^{\frac{4}{3}} & (\xi<0.02)\\ 0.819\,exp(-3.657\xi)+0.097\,exp(-22.3\xi)+0.032\,exp(-57\xi) & (\xi>0.02)\end{cases}$$

where $\xi=\pi DL/Q$, D is the diffusion coefficient of gaseous SA (chosen to be 0.088 cm^{2} s^{-1} from (Hanson and Eisele, 2000)), L is the length of inlet and Q is the sample flow rate. Then:

$$\xi=\frac{\pi DL}{Q}=\frac{3.14\times(0.88\times10^{-4}\ m^{2}\ s^{-1})\times(1.6\ m)}{(7.2\times10^{-3}\div 60\ m^{3}\ s^{-1})}\approx 0.3684>0.02$$

$$\begin{aligned}\eta_{SA,inlet}&=0.819\,exp(-3.657\xi)+0.097\,exp(-22.3\xi)+0.032\,exp(-57\xi)\\&=0.819\,exp(-3.657\times0.3684)+0.097\,exp(-22.3\times0.3684)+0.032\,exp(-57\times0.3684)\\&\approx 0.2129\end{aligned}$$

10) Line 134: Calibration once a month? This is really infrequent! How frequently did they make background measurements?

Response: These set of trace gases monitors are very stable. As shown in Fig. R4, measurement of SO_2, O_3, NO_2, and CO between our BUCT site and surrounding national monitoring stations show a good agreement. So, by doing the multi-point calibration, the data are reliable. And the background measurement is performed along with every calibration experiment by injecting zero air into these instruments.

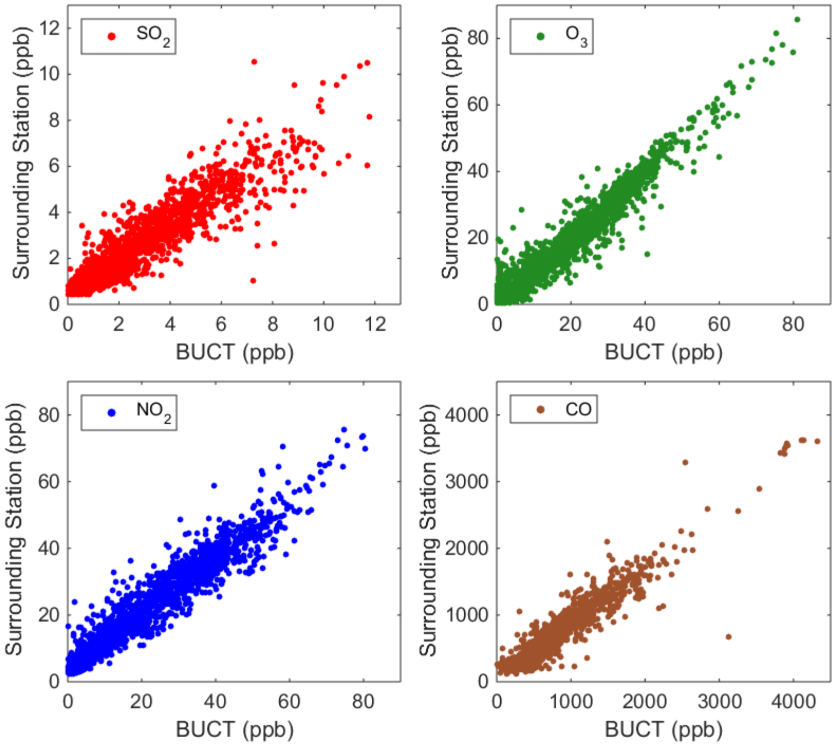

Fig. R4 SO_2, O_3, NO_2, and CO comparison between our BUCT measurement and the averaged data of four surrounding stations (Gucheng, Haidianwanliu, Guanyuan and Wanshouxigong of China National Environmental Monitoring Center). Time period of data are form 1st January to 31st March 2019.

11) Line 143/165: Regardless, SO_2 seemed to me always at the ppb in average, so in high SO_2 conditions year around.

Response: Although the restrict control of SO_2 emission has led to noticeable reduction of SO_2 concentration over the recent years, the concentration of SO_2 remains above ppb level, especially in winter due to the operation of heating system and the low boundary layer height (Fig. R5).

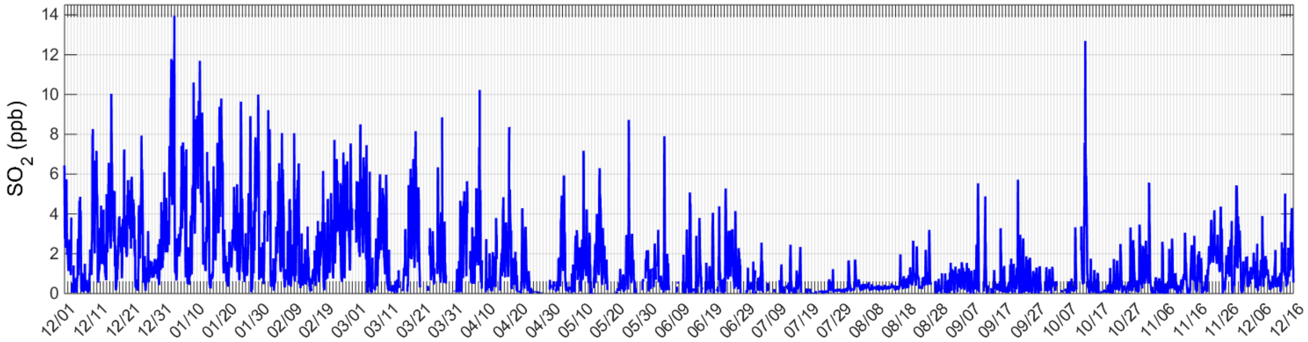

Fig. R5 Time variation of SO_2 from 1st December 2018 to 15th December 2019.

12) Figure 2. Please show amines and ammonia.

Response: Thanks for your suggestion and please also note that Fig. 2 now is Fig. 3.

As we don't have a simultaneous measurements of ammonia (NH_3) and amines, so that we are not able show the NH_3 and amines difference between SA event and non-event nights. Instead, we plotted the diurnal variation from 10th December, 2018 to 6th January, 2019 to show the concentration level of NH_3 and amines as well as the variation between day and night (Fig. R6). Accordingly, the median concentrations of NH_3 and C2+C3 amines are also shown in Table R1.

In general, NH_3 and amines had the highest concentration at night (NH_3 ~3.3 ppb, 8.9×10^{10} cm^{-3}, amines ~ 4.3 ppt, 1.2×10^{8} cm^{-3}) and the lowest concentration at mid-noon (NH_3 ~1.7 ppb, 4.6×10^{10} cm^{-3}, amines ~ 2.3 ppt, 6.2×10^{7} cm^{-3}). Besides, both

NH_3 and amines peaked during the morning rush hour. During nighttime, median NH_3 and amines concentrations were higher under polluted condition (NH_3 ~3.3 ppb, 8.9×10^{10} cm^{-3}, amines ~ 4.1 ppt, 1.1×10^{8} cm^{-3}) that those of Clean-2 condition (NH_3 ~1.9 ppb, 5.1×10^{10} cm^{-3}, amines ~ 2.4 ppt, 6.4×10^{7} cm^{-3}).

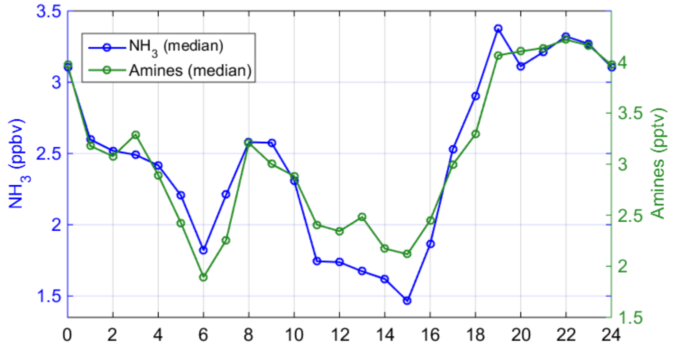

Fig. R6 Diurnal variation of ammonia (NH_3) and C2+C3 amines from 10th December, 2018 to 6th January, 2019.

Table R1 Median concentrations of NH_3 and C2+C3 amines from 10th December, 2018 to 6th January, 2019.

Species	**Unit**	**Night (20:00-04:00)**	**Day (09:00-16:00)**	**Polluted Night (Vis < 12 km)**	**Clean-2 Night (Vis ≥ 16km, [O_3] ≥ 2×10^{11} cm^{-3})**
NH_3	Mixing ratio in ppb	2.8	1.7	3.3	1.9
	Concentration in cm^{-3}	7.6×10^{10}	4.6×10^{10}	8.9×10^{10}	5.1×10^{10}
C2+C3 Amines	Mixing ratio in ppt	3.6	2.3	4.1	2.4
	Concentration in cm^{-3}	9.8×10^{7}	6.2×10^{7}	1.1×10^{8}	6.4×10^{7}

13) Line 191-192: This does not make sense to me.

Response: The sentence in Line 191-192 of the original manuscript is "A good correlation between source and sink suggests that the assumed source and sink processes are the major factors controlling the SA concentration.".

This sentence is used to illustrate the linear correlation between source term and sink term when there are no additional sources (as the case in Fig 5. (b) for Clean-2 condition), but this sentence is indeed confusing when the source term and sink term are not fully explained in advance. Therefore, we decided to remove it from the revised manuscript as the relationship between the source and sink term has been fully discussed in the following part of Section 4.3.

14) Figure s1: move this to the main text – including spring measurements.

Response: Thanks a lot for your suggestion and we have moved Fig. S1 to the main text as Fig. 1. The time variation of spring measurement (from 20th March to 20th May 2019) is shown as Fig. S6 in the revised supplement.

15) Figure s3: the same as Figure 3?

Response: They are not the same. Fig. 3 shows the time variation for nighttime SA events occurred under CS decrease condition, while Fig. S3 displays the time variation for nighttime SA events occurred under SO_2 increase condition. Please also note that, Fig. S3 now is Fig. S2 and Fig. 3 now is Fig. 4.

References

Almeida, J., Schobesberger, S., Kuerten, A., Ortega, I. K., Kupiainen-Maatta, O., Praplan, A. P., Adamov, A., Amorim, A., Bianchi, F., Breitenlechner, M., David, A., Dommen, J., Donahue, N. M., Downard, A., Dunne, E., Duplissy, J., Ehrhart, S., Flagan, R. C., Franchin, A., Guida, R., Hakala, J., Hansel, A., Heinritzi, M., Henschel, H., Jokinen, T., Junninen, H., Kajos, M., Kangasluoma, J., Keskinen, H., Kupc, A., Kurten, T., Kvashin, A. N., Laaksonen, A., Lehtipalo, K., Leiminger, M., Leppa, J., Loukonen, V., Makhmutov, V., Mathot, S., McGrath, M. J., Nieminen, T., Olenius, T., Onnela, A., Petaja, T., Riccobono, F., Riipinen, I., Rissanen, M., Rondo, L., Ruuskanen, T., Santos, F. D., Sarnela, N., Schallhart, S., Schnitzhofer, R., Seinfeld, J. H., Simon, M., Sipila, M., Stozhkov, Y., Stratmann, F., Tome, A., Troestl, J., Tsagkogeorgas, G., Vaattovaara, P., Viisanen, Y., Virtanen, A., Vrtala, A., Wagner, P. E., Weingartner, E., Wex, H., Williamson, C., Wimmer, D., Ye, P., Yli-Juuti, T., Carslaw, K. S., Kulmala, M., Curtius, J., Baltensperger, U., Worsnop, D. R., Vehkamaki, H., and Kirkby, J.: Molecular understanding of sulphuric acid-amine particle nucleation in the atmosphere, Nature, 502, 359-+, 10.1038/nature12663, 2013.

Arnold, F., Pirjola, L., Aufmhoff, H., Schuck, T., Lahde, T., and Hameri, K.: First gaseous sulfuric acid measurements in automobile exhaust: Implications for volatile nanoparticle formation, Atmospheric Environment, 40, 7097-7105, 10.1016/j.atmosenv.2006.06.038, 2006.

Barrios, C. C., Dominguez-Saez, A., Rubio, J. R., and Pujadas, M.: Factors influencing the number distribution and size of the particles emitted from a modern diesel vehicle in real urban traffic, Atmospheric Environment, 56, 16-25, 10.1016/j.atmosenv.2012.03.078, 2012.

Birmili, W., Berresheim, H., Plass-Dulmer, C., Elste, T., Gilge, S., Wiedensohler, A., and Uhrner, U.: The Hohenpeissenberg aerosol formation experiment (HAFEX): a long-term study including size-resolved aerosol, H2SO4, OH, and monoterpenes measurements, Atmospheric Chemistry and Physics, 3, 361-376, 10.5194/acp-3-361-2003, 2003.

Eerdekens, G., Yassaa, N., Sinha, V., Aalto, P. P., Aufmhoff, H., Arnold, F., Fiedler, V., Kulmala, M., and Williams, J.: VOC measurements within a boreal forest during spring 2005: on the occurrence of elevated monoterpene concentrations during night time intense particle concentration events, Atmospheric Chemistry and Physics, 9, 8331-8350, 10.5194/acp-9-8331-2009, 2009.

Erupe, M. E., Benson, D. R., Li, J., Young, L.-H., Verheggen, B., Al-Refai, M., Tahboub, O., Cunningham, V., Frimpong, F., Viggiano, A. A., and Lee, S.-H.: Correlation of aerosol nucleation rate with sulfuric acid and ammonia in Kent, Ohio: An atmospheric observation, Journal of Geophysical Research-Atmospheres, 115, 10.1029/2010jd013942, 2010.

Fiedler, V., Dal Maso, M., Boy, M., Aufmhoff, H., Hoffmann, J., Schuck, T., Birmili, W., Hanke, M., Uecker, J., Arnold, F., and Kulmala, M.: The contribution of sulphuric acid to atmospheric particle formation and growth: a comparison between boundary layers in Northern and Central Europe, Atmospheric Chemistry and Physics, 5, 1773-1785, 10.5194/acp-5-1773-2005, 2005.

Hanson, D. R., and Eisele, F.: Diffusion of H2SO4 in Humidified Nitrogen: Hydrated H2SO4, The Journal of Physical Chemistry A, 104, 1715-1719, 10.1021/jp993622j, 2000.

Iida, K., Stolzenburg, M. R., McMurry, P. H., and Smith, J. N.: Estimating nanoparticle growth rates from size-dependent charged fractions: Analysis of new particle formation events in Mexico City, Journal of Geophysical Research-Atmospheres, 113, 10.1029/2007jd009260, 2008.

Jayne, J. T., Pöschl, U., Chen, Y.-m., Dai, D., Molina, L. T., Worsnop, D. R., Kolb, C. E., and Molina, M. J.: Pressure and Temperature Dependence of the Gas-Phase Reaction of SO3 with H2O and the Heterogeneous Reaction of SO3 with H2O/H2SO4 Surfaces, The Journal of Physical Chemistry A, 101, 10000-10011, 10.1021/jp972549z, 1997.

Kammer, J., Perraudin, E., Flaud, P. M., Lamaud, E., Bonnefond, J. M., and Villenave, E.: Observation of nighttime new particle formation over the French Landes forest, Science of the Total Environment, 621, 1084-1092, 10.1016/j.scitotenv.2017.10.118, 2018.

Kangasluoma, J., Kuang, C., Wimmer, D., Rissanen, M. P., Lehtipalo, K., Ehn, M., Worsnop, D. R., Wang, J., Kulmala, M., and Petaja, T.: Sub-3 nm particle size and composition dependent response of a nano-CPC battery, Atmospheric Measurement Techniques, 7, 689-700, 10.5194/amt-7-689-2014, 2014.

Kirkby, J., Curtius, J., Almeida, J., Dunne, E., Duplissy, J., Ehrhart, S., Franchin, A., Gagne, S., Ickes, L., Kuerten, A., Kupc, A., Metzger, A., Riccobono, F., Rondo, L., Schobesberger, S., Tsagkogeorgas, G., Wimmer, D., Amorim, A., Bianchi, F., Breitenlechner, M., David, A., Dommen, J., Downard, A., Ehn, M., Flagan, R. C., Haider, S., Hansel, A., Hauser, D., Jud, W., Junninen, H., Kreissl, F., Kvashin, A., Laaksonen, A., Lehtipalo, K., Lima, J., Lovejoy, E. R., Makhmutov, V., Mathot, S., Mikkila, J., Minginette, P., Mogo, S., Nieminen, T., Onnela, A., Pereira, P., Petaja, T., Schnitzhofer, R., Seinfeld, J. H., Sipila, M., Stozhkov, Y., Stratmann, F., Tome, A., Vanhanen, J., Viisanen, Y., Vrtala, A., Wagner, P. E., Walther, H., Weingartner, E., Wex, H., Winkler, P. M., Carslaw, K. S., Worsnop, D. R., Baltensperger, U., and Kulmala, M.: Role of sulphuric acid, ammonia and galactic cosmic rays in atmospheric aerosol nucleation, Nature, 476, 429-U477, 10.1038/nature10343, 2011.

Kontkanen, J., Lehtipalo, K., Ahonen, L., Kangasluoma, J., Manninen, H. E., Hakala, J., Rose, C., Sellegri, K., Xiao, S., Wang, L., Qi, X., Nie, W., Ding, A., Yu, H., Lee, S., Kerminen, V.-M., Petaja, T., and Kulmala, M.: Measurements of sub-3nm particles using a particle size magnifier in different environments: from clean mountain top to polluted megacities, Atmospheric Chemistry and Physics, 17, 2163-2187, 10.5194/acp-17-2163-2017, 2017.

Kuerten, A., Bergen, A., Heinritzi, M., Leiminger, M., Lorenz, V., Piel, F., Simon, M., Sitals, R., Wagner, A. C., and Curtius, J.: Observation of new particle formation and measurement of sulfuric acid, ammonia, amines and highly oxidized organic molecules at a rural site in central Germany, Atmospheric Chemistry and Physics, 16, 12793-12813, 10.5194/acp-16-12793-2016, 2016.

Kulkarni, P., Baron, P. A., and Willeke, K.: Aerosol measurement: principles, techniques, and applications, John Wiley & Sons, 2011.

Kurten, A., Rondo, L., Ehrhart, S., and Curtius, J.: Calibration of a Chemical Ionization Mass Spectrometer for the Measurement of Gaseous Sulfuric Acid, Journal of Physical Chemistry A, 116, 6375-6386, 10.1021/jp212123n, 2012.

Lehtipalo, K., Sipila, M., Junninen, H., Ehn, M., Berndt, T., Kajos, M. K., Worsnop, D. R., Petaja, T., and Kulmala, M.: Observations of Nano-CN in the Nocturnal Boreal Forest, Aerosol Science and Technology, 45, 499-509, 10.1080/02786826.2010.547537, 2011.

Lehtipalo, K., Yan, C., Dada, L., Bianchi, F., Xiao, M., Wagner, R., Stolzenburg, D., Ahonen, L. R., Amorim, A., Baccarini, A., Bauer, P. S., Baumgartner, B., Bergen, A., Bernhammer, A.-K., Breitenlechner, M., Brilke, S., Buchholz, A., Mazon, S. B., Chen, D., Chen, X., Dias, A., Dommen, J., Draper, D. C., Duplissy, J., Ehn, M., Finkenzeller, H., Fischer, L., Frege, C., Fuchs, C., Garmash, O., Gordon, H., Hakala, J., He, X., Heikkinen, L., Heinritzi, M., Helm, J. C., Hofbauer, V., Hoyle, C. R., Jokinen, T., Kangasluoma, J., Kerminen, V.-M., Kim, C., Kirkby, J., Kontkanen, J., Kuerten, A., Lawler, M. J., Mai, H., Mathot, S., Mauldin, R. L., III, Molteni, U., Nichman, L., Nie, W., Nieminen, T., Ojdanic, A., Onnela, A., Passananti, M., Petaja, T., Piel, F., Pospisilova, V., Quelever, L. L. J., Rissanen, M. P., Rose, C., Sarnela, N., Schallhart, S., Schuchmann, S., Sengupta, K., Simon, M., Sipila, M., Tauber, C., Tome, A., Trostl, J., Vaisanen, O., Vogel, A. L., Volkamer, R., Wagner, A. C., Wang, M., Weitz, L., Wimmer, D., Ye, P., Ylisirnio, A., Zha, Q., Carslaw, K. S., Curtius, J., Donahue, N. M., Flagan, R. C., Hansel, A., Riipinen, I., Virtanen, A., Winkler, P. M., Baltensperger, U., Kulmala, M., and Worsnop, D. R.: Multicomponent new particle formation from sulfuric acid, ammonia, and biogenic vapors, Science Advances, 4, 10.1126/sciadv.aau5363, 2018.

McMurry, P. H., Fink, M., Sakurai, H., Stolzenburg, M. R., Mauldin, R. L., Smith, J., Eisele, F., Moore, K., Sjostedt, S., Tanner, D., Huey, L. G., Nowak, J. B., Edgerton, E., and Voisin, D.: A criterion for new particle formation in the sulfur-rich Atlanta atmosphere, Journal of Geophysical Research-Atmospheres, 110, 10.1029/2005jd005901, 2005.

Paasonen, P., Nieminen, T., Asmi, E., Manninen, H. E., Petaja, T., Plass-Duelmer, C., Flentje, H., Birmili, W., Wiedensohler, A., Horrak, U., Metzger, A., Hamed, A., Laaksonen, A., Facchini, M. C., Kerminen, V. M., and Kulmala, M.: On the roles of sulphuric acid and low-volatility organic vapours in the initial steps of atmospheric new particle formation, Atmospheric Chemistry and Physics, 10, 11223-11242, 10.5194/acp-10-11223-2010, 2010.

Ronkko, T., Kuuluvainen, H., Karjalainen, P., Keskinen, J., Hillamo, R., Niemi, J. V., Pirjola, L., Timonen, H. J., Saarikoski, S., Saukko, E., Jarvinen, A., Silvennoinen, H., Rostedt, A., Olin, M., Yli-Ojanpera, J., Nousiainene, P., Kousa, A., and Dal Maso, M.: Traffic is a major source of atmospheric nanocluster aerosol, Proceedings of the National Academy of Sciences of the United States of America, 114, 7549-7554, 10.1073/pnas.1700830114, 2017.

Rose, C., Zha, Q., Dada, L., Yan, C., Lehtipalo, K., Junninen, H., Mazon, S. B., Jokinen, T., Sarnela, N., Sipila, M., Petaja, T., Kerminen, V.-M., Bianchi, F., and Kulmala, M.: Observations of biogenic ion-induced cluster formation in the atmosphere, Science Advances, 4, 10.1126/sciadv.aar5218, 2018.

Slater, E. J., Whalley, L. K., Woodward-Massey, R., Ye, C., Lee, J. D., Squires, F., Hopkins, J. R., Dunmore, R. E., Shaw, M., Hamilton, J. F., Lewis, A. C., Crilley, L. R., Kramer, L., Bloss, W., Vu, T., Sun, Y., Xu, W., Yue, S., Ren, L., Acton, W. J. F., Hewitt, C. N., Wang, X., Fu, P., and Heard, D. E.: Elevated levels of OH observed in haze events during wintertime in central Beijing, Atmos. Chem. Phys. Discuss., 2020, 1-43, 10.5194/acp-2020-362, 2020.

Vanhanen, J., Mikkila, J., Lehtipalo, K., Sipila, M., Manninen, H. E., Siivola, E., Petaja, T., and Kulmala, M.: Particle Size Magnifier for Nano-CN Detection, Aerosol Science and Technology, 45, 533-542, 10.1080/02786826.2010.547889, 2011.

Wang, Z. B., Hu, M., Yue, D. L., Zheng, J., Zhang, R. Y., Wiedensohler, A., Wu, Z. J., Nieminen, T., and Boy, M.: Evaluation on the role of sulfuric acid in the mechanisms of new particle formation for Beijing case, Atmospheric Chemistry and Physics, 11, 12663-12671, 10.5194/acp-11-12663-2011, 2011.

Yao, L., Garmash, O., Bianchi, F., Zheng, J., Yan, C., Kontkanen, J., Junninen, H., Mazon, S. B., Ehn, M., Paasonen, P., Sipila, M., Wang, M. Y., Wang, X. K., Xiao, S., Chen, H. F., Lu, Y. Q., Zhang, B. W., Wang, D. F., Fu, Q. Y., Geng, F. H., Li, L., Wang, H. L., Qiao, L. P., Yang, X., Chen, J. M., Kerminen, V. M., Petaja, T., Worsnop, D. R., Kulmala, M., and Wang, L.: Atmospheric new particle formation from sulfuric acid and amines in a Chinese megacity, Science, 361, 278-+, 10.1126/science.aao4839, 2018.

Formation of Nighttime Sulfuric Acid from the Ozonolysis of Alkenes in Beijing

Yishuo Guo[1], Chao Yan[1,2,*], Chang Li[1], Zemin Feng[1], Ying Zhou[1], Zhuohui Lin[1], Lubna Dada[2], Dominik Stolzenburg[2], Rujing Yin[3], Jenni Kontkanen[2], Kaspar R. Daellenbach[2], Juha Kangasluoma[1,2], Lei Yao[2], Biwu Chu[2], Yonghong Wang[2], Runlong Cai[2], Federico Bianchi[2], Yongchun Liu[1] and Markku Kulmala[1,2]

[1] Aerosol and Haze Laboratory, Beijing Advanced Innovation Center for Soft Matter Science and Engineering, Beijing University of Chemical Technology, Beijing, China

[2] Institute for Atmospheric and Earth System Research / Physics, Faculty of Science, University of Helsinki, Finland

[3] State Key Joint Laboratory of Environment Simulation and Pollution Control, State Environmental Protection Key Laboratory of Sources and Control of Air Pollution Complex, School of Environment, Tsinghua University, Beijing, China

**Correspondence to*: Chao Yan (chao.yan@helsinki.fi)

Abstract. Gaseous sulfuric acid (SA) has received a lot of attention for its crucial role in atmospheric new particle formation (NPF), and for this reason, studies until now have mainly focused on daytime SA when most NPF events occur. While daytime SA production is driven by SO_2 oxidation of OH radical from photochemical origin, the formation of SA during night and its potential influence on particle formation remains poorly understood. Here we present evidence for significant nighttime SA production in urban Beijing during winter, yielding concentrations between 1.0 and 3.0×10^6 cm^{-3}. We found a high frequency (~ 30%) of nighttime SA events, which are defined by the appearance of a distinct SA peak observed between 20:00 and 04:00 local time, and with the maximum concentration exceeding 1.0×10^6 cm^{-3}. These events mostly occurred during unpolluted nights with low vapor condensation sink. Furthermore, we found that under very clean conditions (visibility > 16.0 km) with abundant ozone (concentration > 2.0×10^{11} cm^{-3}, ~ 7 ppb), the overall sink of SA was strongly correlated with the products of O_3, alkenes and SO_2 concentrations, suggesting that the ozonolysis of alkenes played a major role in nighttime SA formation under such conditions. This is in light with previous studies showing that the ozonolysis of alkenes can form OH radical and stabilized Criegee intermediate (sCI), both of which are able to oxidize SO_2 leading to SA formation. However, we also need to point out that there exist additional sources of SA under more polluted condition, which are not investigated in this study. Moreover, there was a strong correlation between SA concentration and the number concentration of sub-3 nm particles in both clean and polluted nights. Different from forest environments, where oxidized biogenic vapors are the main driver of nighttime clustering, our study demonstrates that the formation of nighttime cluster mode particles in urban environments is mainly driven by nighttime SA production.

Keywords: nighttime SA, urban environment, ozonolysis of alkenes, sub-3 nm particles

1. Introduction

Atmospheric aerosol particles have considerable impact on global climate by directly affecting the radiation balance of the earth and by indirectly acting as cloud condensation nuclei (Stocker et al., 2014). The number concentration of these aerosol particles depends to a large extent on the atmospheric new particle formation (NPF), which includes gas-phase nucleation and subsequent growth of newly formed particles. Studies over the past twenty years have shown that the SA is the major gaseous precursor of NPF in most environments inside the continental boundary layer (Lee et al., 2019). Sulfuric acid driven NPF can proceed as SA-water binary nucleation, SA-water-ammonia ternary nucleation (Kirkby et al., 2011), SA-amine-water nucleation (Almeida et al., 2013;Kuerten et al., 2014), SA-organics nucleation (Riccobono et al., 2014), and SA-organics-amonia nucleation (Lehtipalo et al., 2018) and H_2SO_4-H_2O-NH_3-amine nucleation (Myllys et al., 2019;Yu et al., 2012). Both the nucleation rate (J_{nuc}) and the initial growth rate of newly formed particles tends to have a power-law relationship with the SA concentration: $J_{nuc} = k \times SA^{\alpha}$, where the activation nucleation is dominant when $\alpha \approx 1$ (Kulmala et al., 2006), the kinetic nucleation is dominant when $\alpha \approx 2$ (Riipinen et al., 2007;Paasonen et al., 2009;Erupe et al., 2010) and the thermodynamic nucleation becomes more crucial when α is larger than 2.5 (Wang et al., 2011).

Due to the importance of SA for NPF, accurate and reliable measurement of SA is of great importance. Up to now, ambient SA concentrations have been reported for many sites (Weber et al., 1997;Weber et al., 1998;Weber et al., 1999;Paasonen et al., 2010;Jokinen et al., 2018;Fiedler et al., 2005;Eisele et al., 2006;Boy et al., 2008;Iida et al., 2008;Wang et al., 2011;Kuerten et al., 2016;Yao et al., 2018;Mauldin et al., 2001;Erupe et al., 2010;Yu et al., 2014). These studies indicate that the concentration level of SA in the atmosphere is closely related to human activities. In general, daytime SA concentration is around 10^5 cm^{-3} in pristine Antarctica region (Mauldin et al., 2001), 10^6 cm^{-3} in remote continental, remote marine and forest regions (which are less affected by human activities) and 10^7 cm^{-3} in urban and rural agricultural lands (which are influenced dominantly by human activities (Birmili et al., 2003;Fiedler et al., 2005;McMurry et al., 2005;Iida et al., 2008;Erupe et al., 2010;Paasonen et al., 2010;Wang et al., 2011;Yao et al., 2018)). SA generally shows a distinct diurnal pattern correlating with radiation (Lu et al., 2019) with typical concentrations between 10^6 to 10^7 cm^{-3} during daytime and 10^4 to 10^6 cm^{-3} during nighttime. The seasonal variation of SA is only reported in very few studies, showing higher concentrations during spring and summer than in winter and autumn (Erupe et al., 2010).

Due to the strong connection between SA and NPF, previous studies mostly focused on understanding the SA formation in the daytime. However, recent observation on the formation of sub-3 nm particles have shown that these cluster mode particles also exist with high concentration during the night (Junninen et al., 2008;Lehtipalo et al., 2011;Kulmala et al., 2013;Kecorius et al., 2015;Mazon et al., 2016;Yu et al., 2014) and sometimes even nighttime particle nucleation events can be clearly distinguished. In boreal forest environments, nighttime cluster formation can be attributed to highly oxygenated organic molecules (HOMs) (Kammer et al., 2018;Rose et al., 2018). However, the sources of SA and its role in the particle formation during the nighttime remain largely unresolved, both of which are the focus of this work. In this study, we show noticeable nighttime sulfuric acid sometimes increase of SA during the nighttime in urban Beijing. We further investigate the main sources of SA and demonstrate its role in the nocturnal formation of sub-3nm clusters.

2. Nighttime Sulfuric Acid Formation

During the daytime, gaseous SA is primarily a photochemical product generated from the oxidation of SO_2 by OH radical, while at nighttime, SA is highly associated with non-photochemical oxidants, most likely the non-photochemical OH radical and stabilized Criegee intermediate (sCI) (Mauldin et al., 2012;Taipale et al., 2014). And that non-photochemical SA formation pathway has been investigated in the boreal forest environment (Dada et al., 2020). The non-photochemical oxidation pathway mainly includes the following five reactions. First, the production of (stabilized) Criegee Intermediates by the ozonolysis of alkenes:

$$\mathrm{Alkene} + \mathrm{O_3} \xrightarrow{k_1} \varphi\mathrm{sCI} + (1-\varphi)\mathrm{CI} + \mathrm{RCHO} \qquad \mathrm{R1}$$

Then, the direct oxidation of SO_2 by long lived sCI:

$$\mathrm{sCI} + \mathrm{SO_2} \xrightarrow{k_2} \mathrm{SO_3} + \mathrm{RCHO} \qquad \mathrm{R2}$$

Or the alternative oxidation of SO_2 by OH radicals formed from decomposition of (stabilized) Criegee Intermediates:

$$\mathrm{sCI} \xrightarrow{k_3} \cdot\mathrm{OH} + \mathrm{R_1COR_2} \qquad \mathrm{R3}$$

$$\mathrm{CI} \xrightarrow{k_4} \cdot\mathrm{OH} + \mathrm{R_1COR_2} \qquad \mathrm{R4}$$

$$\mathrm{SO_2} + \cdot\mathrm{OH} + \mathrm{O_2} \xrightarrow{k_5} \mathrm{HO_2}\cdot + \mathrm{SO_3} \qquad \mathrm{R5}$$

where k_i is the rate constant of each reaction, φ is the yield of sCI in the ozonolysis of alkenes, and CI is the chemically activated Criegee intermediate. The lifetime of SO_3 due to its fast reaction with H_2O to form SA is approximately 2×10^{-4} s (see detailed calculation in supplement Section S1), which indicates that this reaction is so fast that almost all SO_3 will be instantaneously converted to SA. In this case, the oxidation of SO_2 is the rate-limiting step in the formation of SA. Currently, only limited types of sCI has been studied: isoprene-derived sCI (Neeb et al., 1997;Zhang et al., 2002;Atkinson et al., 2006;Newland et al., 2015b), monoterpene-derived sCI (Hatakeyama et al., 1984;Rickard et al., 1999;Zhang and Zhang, 2005;Mauldin et al., 2012;Sipila et al., 2014;Vereecken et al., 2017) and the simplest sCI including CH_2COO, CH_3CHOO and $(CH_3)_2COO$ (Hatakeyama et al., 1984;Hasson et al., 2001;Welz et al., 2012;Taatjes et al., 2013;Welz et al., 2014;Newland et al., 2015a;Vereecken et al., 2017). Based on the aforementioned studied, the yield φ of sCI can vary from 0.1 to 0.65 and the rate constants for different reactions span over several orders of magnitude, for k_1 from 1.6×10^{-18} to 2.5×10^{-16} $\mathrm{cm^3s^{-1}}$ and for k_2 from 1.4×10^{-13} to $2.2 \times 10^{-10}\mathrm{cm^3s^{-1}}$. The yield of OH radical from ozonolysis of different type of alkenes also covers a wide range with values of 0.68 – 0.91, 0.24 – 0.35, 0.25 – 0.44, 0.32 – 0.40 and 0.33 – 1.00 for α-pinene, β-pinene, isoprene, propene and other C4-C6 alkenes respectively (Atkinson et al., 1992;Aschmann, 1993;Chew and Atkinson, 1996;Rickard et al., 1999;Siese et al., 2001;Witter et al., 2002;Berndt et al., 2003;Aschmann et al., 2003;Nguyen et al., 2009;Malkin et al., 2010). Moreover, the bimolecular reaction and decomposition reactivity of sCI is highly structure-dependent. sCI with more complicated substituent groups tend to react with H_2O more slowly (Huang et al., 2015), decompose faster (Fenske et al., 2000;Hasson et al., 2001) and more likely to react with SO_2. There were also studies showing that the reactions between sCI and SO_2 were pressure and temperature dependent and were commonly affected by the presence of water and other constituents (Kotzias et al., 1990;Sipila et al., 2014).

3. Ambient Observations

The continuous and comprehensive measurements were conducted at the west campus of Beijing University of Chemical Technology (39.95 °N′, 116.31 °E′). Here we investigate the time period from 18th January to 16th March 2019. The measuring instruments are located on the fifth floor, which is about 15 m above the ground level. This station is a typical urban site, which is around 130 m to the nearest Zizhuyuan Road, 550 m to the West Third Ring Road, and surrounded by commercial properties and residential dwellings.

3.1 Measurement of Sulfuric Acid with CI-APi-TOF

Sulfuric acid is measured by a long time-of-flight chemical ionization mass specter (LTOF-CIMS, Aerodyne Research, Inc.) equipped with a nitrate chemical ionization source. The basic working principle of this instrument can be found elsewhere (Jokinen et al., 2012). In our measurement, we draw air through a stainless-steel tube with a length of 1.6 m and a diameter of 3/4 inch with a flowrate at 7.2 L min^{-1}. In addition, we have implemented a flush plate (Karsa Inc.) to effectively remove water molecules entering the instrument, which is found necessary to maintain a continuous measurement.

The quantification of sulfuric acid is derived from the ratio of bisulfate ions (with counting rates unit in ions·s^{-1}) relative to primary ions as follows:

$$[\mathrm{H_2SO_4}] = \frac{\mathrm{HSO_4^-} + \mathrm{H_2SO_4NO_3^-}}{\mathrm{NO_3^-} + \mathrm{HNO_3NO_3^-} + (\mathrm{HNO_3})_2\mathrm{NO_3^-}} \times \mathrm{C}$$

The calibration factor, C, is determined from direct calibration by injecting gaseous sulfuric acid of known amounts into the instrument (Kurten et al., 2012). The diffusional wall loss of the 1.6 sampling line is 0.2423, and after taking into account of it, we a value of 6.07×10^9 cm^{-3} as the final calibration coefficient.

3.2 Measurement of Alkenes with SPI-MS

Six alkenes are analyzed in this study, i.e., including propylene, butylene, butadiene, isoprene, pentene and hexene, which were detected by a single photon ionization time-of-flight mass spectrometer (SPI-MS 3000, Guangzhou Hexin Instrument Co., Ltd., China) (Gao et al., 2013). It should be mentioned that this instrument cannot distinguish conformers, and therefore the pentene and haxene could also be cyclopentane and cyclohexane, respectively. A polydimethylsiloxane (PDMS) membrane sampling system is used. As the PDMS membrane has better selective adsorption to volatile organic compounds (VOCs), VOC molecules can be concentrated after diffusing and desorbing from the membrane under vacuum sampling condition. In this way, the detection limit of VOCs can be improved. Then the gas molecules are guided to an ionization chamber through a 2 mm-diameter stainless steel capillary, where VOC molecules are ionized by the vacuum ultraviolet (VUV) light with an ionization energy smaller than 10.8eV. For the detection of positive ions, two microchannel plates (MCPs, Hamamatsu, Japan) assembled with a chevron-type configuration are employed. An analog to digital converter (ADC) was used to measure and record the output current signal from the MCPs.

Alkenes concentrations are quantified by performing a direct calibration. The PAMS (Photochemical Assessment Monitoring Stations) and TO-15 environmental gases (including 57 and 65 types of VOCs separately, Linde Gas North America LLC, USA) are used as two standard gases with ultra-high-purity nitrogen as the carrier gas. Gas with different concentrations of VOC standards is produced by mixing a constant carrier gas with standard gas of varying flow rates. The calibration coefficient is further calculated from the ratio between the actual concentration and the ion intensity.

3.3 Other Ancillary Measurements

The number concentration of clusters with the size range of 1.30~2.45 nm was measured with a Particle Sizer Magnifier (PSM) (Vanhanen et al., 2011), and the integrated number concentration of particles from PSM is referred as $N_{Sub\text{-}3nm}$ in the following. The number size distributions of aerosol particles from 6 to 840 nm and from 0.52 to 19.81 μm are measured by the Differential Mobility Particle Sizer (DMPS) (Aalto et al., 2001) and the Aerodynamic Particle Sizer (APS) (Armendariz and Leith, 2002) respectively. Meteorological parameters are measured with a weather station (AWS310, Vaisala Inc.) located on the rooftop of the building. These parameters include the ambient temperature, relative humidity (RH), pressure, visibility, UVB radiation, as well as horizontal wind speed and direction. Trace gas concentrations of carbon monoxide (CO), sulfur dioxide (SO_2) nitrogen oxides (NO_x) and ozone (O_3) are monitored using four Thermo Environmental Instruments (models 48i, 43i-TLE, 42i, 49i, respectively). Calibration of these instruments are performed monthly using the standard gases of known concentrations. The mass concentration of $PM_{2.5}$ is directly measured with a Tapered Element Oscillating Microbalance Dichotomous Ambient Particulate Monitor (TEOM 1405-DF, Thermo Fisher Scientific Inc, USA) with a total flow rate of 16.67 L/min. In addition, the loss rate of gas-phase sulfuric acid described by condensation sink (CS) is calculated based on the size distribution data from DMPS and APS (Kulmala et al., 2001).

4. Results and Discussions

4.1 Definition of Nighttime Sulfuric Acid Event

An overview of our measurements during 18th January to 16th March 2019 is shown in Fig. 1. As our measurement period overlaps with the heating period in Beijing (from 15th November 2018 to 15th March 2019), the SO_2 level during the measurement period was higher than that of other periods in one year (from 16th March to 31st May 2019) (Fig. S1 in the Supplement).

In this work, the nighttime window is defined between 20:00 and 04:00 (following day) to exclude any possible influence of photochemistry. Fig. 2 shows the diurnal variation of SA concentration on one typical SA event night (14 March 2019) and one typical SA non-event night (3 February 2019). Overall, nighttime SA concentrations vary between 3.0×10^5 and 3.0×10^6

cm^{-3} in our measurement period. The nighttime event in Fig. 2 shows a distinct SA peak at around 22:00 with a maximum SA concentration of around 3.0×10^{6} cm^{-3}, which is almost half of the daily maximum value. While in the non-event case, SA continues decreasing throughout the evening, reaching a minimal value of 3.0×10^{5} cm^{-3}. A nighttime SA event is defined when both of the following two criteria are both met: (a) there is a distinct peak during the nighttime hours, (b) the SA concentration exceeds 1.0×10^{6} cm^{-3}. The nights without distinct peaks are classified as SA non-event nights, and if a peak is identified but it does not meet criterion (b), the night is classified as an undefined night. Out of all 56 nights studied, there are in total 18 SA event nights, 16 non-event nights, and 22 undefined nights (listed in Table. S1). Thus, the overall frequency of nighttime SA events during our observation period is 32%, which means that nearly a third of nights during our observation period had distinct nighttime sulfuric acid peaks.

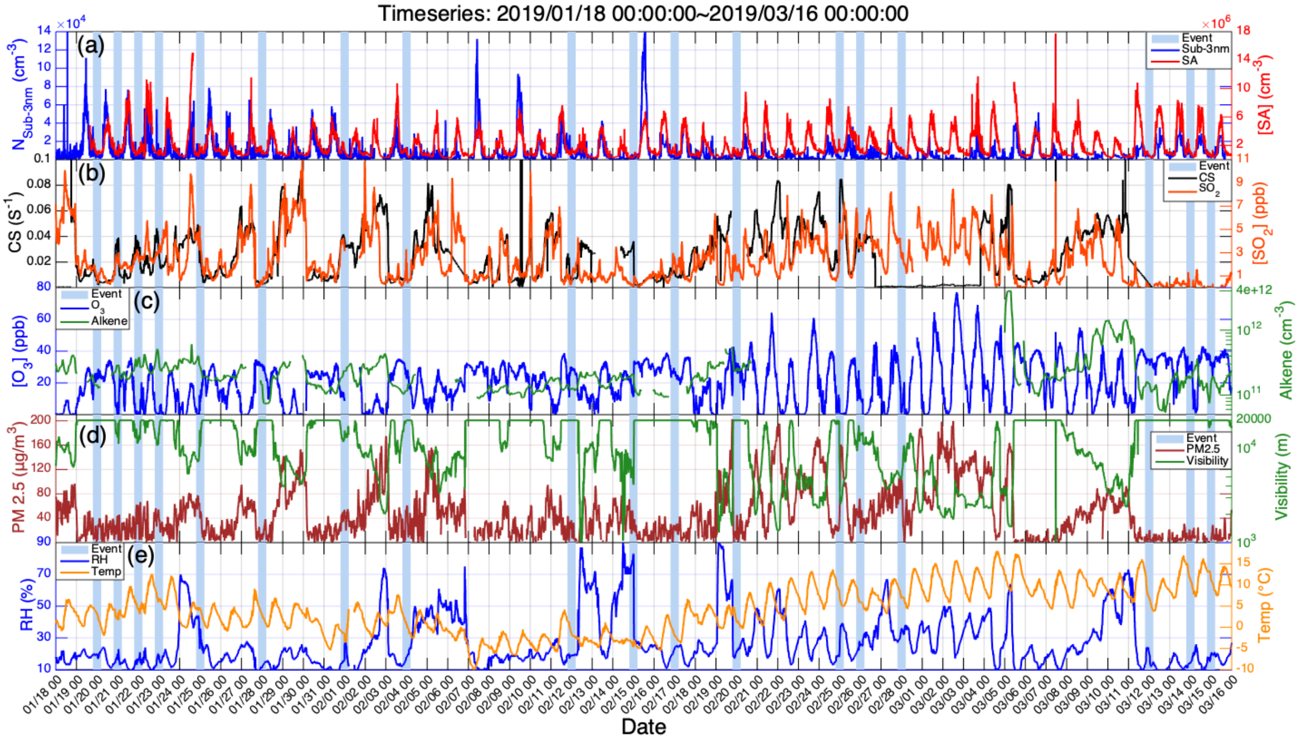

Fig. 1 Overview of different parameters measured from 18th January, 2019 to and 16th March, 2019 for (a) SA concentration and particle number concentration of sub-3nm particles (N$_{\text{Sub-3nm}}$, measured by PSM), (b) CS and SO$_2$ concentration, (c) concentration of O$_3$ and Alkenes, (d) PM$_{2.5}$ and visibility, and (e) relative humidity (RH) and temperature. The light blue bars represent nights with nighttime SA events.

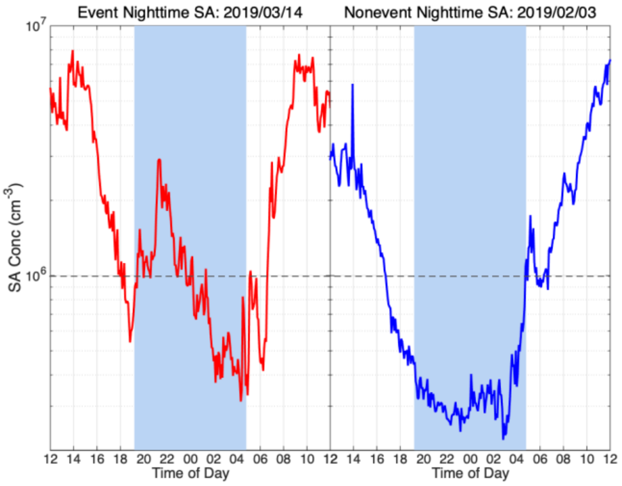

Fig. 2 Daily variation of SA concentration on a typical night with a nighttime SA event (red line, 14th March, 2019) and on a non-event night (blue line, 3rd February, 2019). The shaded blue area shows the period that is considered as nighttime in this study.

4.2 Features of Nighttime Sulfuric Acid Event

We further analyzed the features of nighttime SA event nights based on the above mentioned 18 event nights and 16 non-event nights (Fig. 3). On SA event nights, the mass concentration of $PM_{2.5}$, the mixing ratio of NO_x, CS and RH were clearly lower, and visibility was clearly higher than on non-event nights. This suggests that nighttime SA events tend to occur under clean conditions. In addition, higher concentrations of O_3 were associated with SA event nights, whereas the concentration of SO_2 did not vary as much between SA event and non-event nights. This indicates that at most of the time, the concentration of SO_2 is not the dominant factor that explains the variation of nighttime SA.

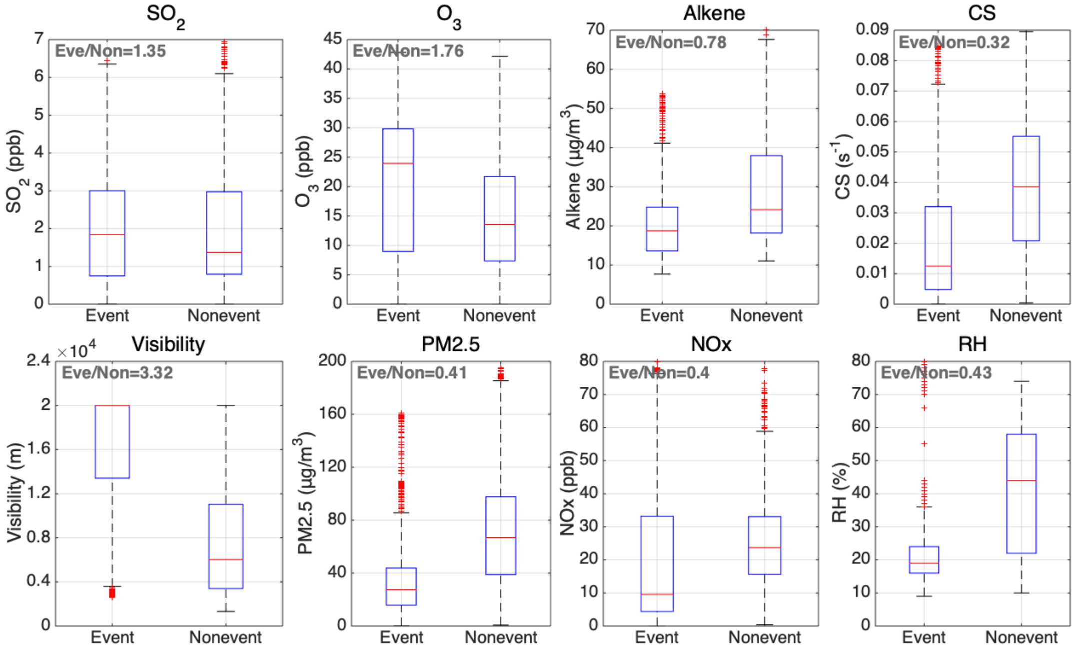

Fig. 3 Boxplots for the concentrations of SO_2, O_3 and alkenes, CS, visibility, $PM_{2.5}$, NO_x concentration and RH during nighttime SA event and non-event nights. In each plot, the red line is the median value, the bottom and the top blue lines are the 25 and 75 percentiles, and the whisker range covers the ± 2.7σ of the data. Outliers are the ones out of the ± 2.7σ range of all selected data. The dark gray values on the top left corners are the ratios between median values of event and non-event days.

We further investigated the determining factor for the occurrence of SA events by looking into different variables during the SA event nights. CS measurements were available for 13 event nights, during which 15 SA peaks were observed. In general, we found that eight events (53%) were mainly associated with the decrease of CS. This is demonstrated in Fig. 4, where the nighttime events as well as the simultaneous decrease of CS are highlighted with green dots. Four other cases (27%) were mostly due to the increase of SO_2 concentration (Fig. S2), and the remaining three cases were likely synergistically caused by SO_2, O_3, alkenes, CS and other parameters. More details are provided in Table S2.

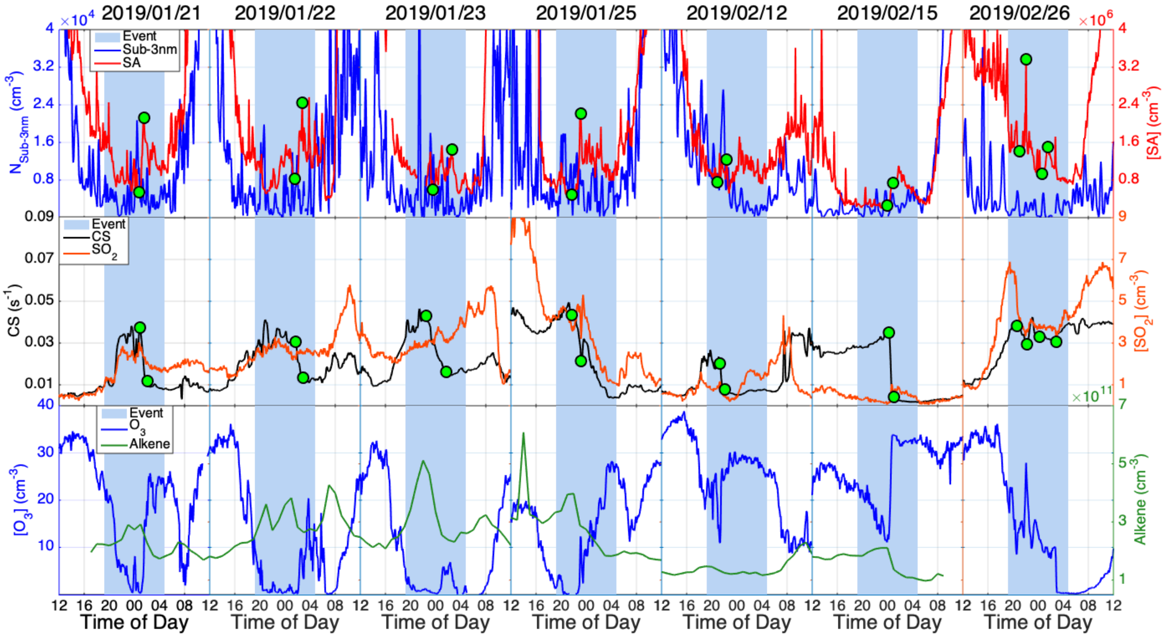

Fig. 4 Daily time-series of different variables on nighttime SA event days when SA events occurred under CS decrease conditions. The top panel shows the $N_{\mathrm{Sub\text{-}3nm}}$ and SA concentration, the middle panel shows CS and SO_2 concentration, and the bottom panel shows the concentration of O_3 and alkenes. Green dots show times when CS started to drop and reached its minimum value.

4.3 Source and Sink Balance for Nighttime Sulfuric Acid: Importance of Alkene Ozonolysis

As discussed above, nighttime SA events mainly occurred under clean conditions with low CS values. Therefore, we classified all the nighttime data set into three groups according to the air pollution level, which is assessed by visibility. The division standards for pollution level is explained in detail in Section S3. The clean (named Clean-1), mildly polluted and heavy polluted conditions are defined by visibility values which are larger than 12.0 km, in the range of 4.0 - 12.0 km and smaller than 4.0 km respectively. Accordingly, data points under each condition took up 48%, 25% and 27% of all data points.

After classifying the data set into groups based on the pollution level, the balance between SA source and sink for each group was investigated separately. The ozonolysis of alkenes under dark conditions is capable of generating sCI as well as OH radical, both of which are able to oxidize SO_2 to form gaseous SA. However, the yields of both sCI and recycled OH radical remain largely unquantified. Therefore, we do not attempt to distinguish the contribution of sCI and OH radical on SA formation in this study, but rather treat them as a "bulk oxidant" and use an empirical parameter k_{app} to account for both oxidation pathways. Accordingly, the source term (production rate) of SA can be expressed as $k_{app}\cdot[SO_2]\cdot[O_3]\cdot[\mathrm{Alkene}]$, where k_{app} is an overall empirical parameter that takes into account the yields of OH radical and sCI as well as the rate constants of their reactions with SO_2. The sink term (loss rate) consists of two parts: the condensation of SA onto particles ($[SA]\cdot CS$) and the collision of SA monomers with each other to form SA dimers ($\beta\cdot[SA]^2$). In reality, SA monomer also collides with SA dimers and larger clusters, but due to the low concentration of SA clusters, those collisions are negligible compared to other losses. In a polluted environment where strong stabilizers of SA exist, the formation rate of stable SA dimer is close to the collision limit (Yao et al., 2018). Therefore, β can be taken as the hard-sphere collision rate, which is calculated to be 3.46×10^{-10} $cm^3\ s^{-1}$ (Seinfeld and Pandis, 2016). Under pseudo-steady-state (PSS) assumption (see Section S2 for detailed disscussion about PSS assumption), the source-sink balance of SA can be expressed as follows:

$$\mathrm{k_{app}} \cdot [\mathrm{Alkene}] \cdot [\mathrm{O_3}] \cdot [\mathrm{SO_2}] = [\mathrm{SA}] \cdot \mathrm{CS} + \beta \cdot [\mathrm{SA}]^2$$

Fig. 5 shows the nighttime correlation between SA source term and sink term under different pollution levels, with the data binned by SA sources. If the source and the sink term correlate, then the slope represents the overall apparent rate constant (k_{app}) concerning the reaction between oxidants (OH radical and sCI) from ozonolysis of alkenes and SO_2 for this specific pollution level.

Under Clean-1 conditions (Fig. 5 (a)), the source term and sink term have a good linear correlation (R^2=0.97) in the source range of 1.0×10^{33} - 4.5×10^{33} $(cm^{-3})^3$, while the balance is broken up outside of this range. These uncorrelated data points outside of this range appear when the visibility was smaller than 16.0 km (Fig. S4 (a)) along with higher concentrations of NO_x and NO ($[NO_x] >$ ~ 40 ppb, Fig. S4 (b) and ($[NO] >$ ~ 3 ppb, Fig. S4 (c)). High NO_x levels always relate to pollution, and NO will consume O_3, leading to much lower O_3 concentration (marked by blue empty circles in Fig. S4 (a)). Thus, we redefined the criterion for clean condition (Clean-2) so that visibility needs to be larger than 16.0 km and O_3 concentration higher than 2.0×10^{11} cm^{-3} (~ 7 ppb). These conditions account for 38% of all data. Fig. 5 (b) shows the good correlation between $[SO_2]\cdot[O_3]\cdot[\mathrm{Alkene}]$ source term and $[SA]\cdot CS+\beta\cdot[SA]^2$ sink term (R^2=0.97) under the redefined clean condition over the entire source range. This suggests that the ozonolysis of alkenes indeed have a dominant contribution to the formation of SA during nighttime under very clean conditions. Generally, the sink term of SA condensation onto particles took up 95.5% for Clean-2 condition and increase to 99.7% for heavy polluted condition. The fitted value, 95% confidence bounds, uncertainty of k_{app} and correlation coefficient R^2 for Clean-1and Clean-2 condition are listed in Table S3.

If we compare the SA source and sink correlation between the Clean-1 (Fig. 5 (a)) and Clean-2 (Fig. 5 (b)) condition, it is obvious that the slope of the linear region of Clean-1 condition data points (2.7×10^{-30} cm^6 s^{-2}) matches well with the slope of Clean-2 condition data points (2.6×10^{-30} cm^6s^{-2}), which further confirms the reliability of the balance between $[SO_2]\cdot[O_3]\cdot[\mathrm{Alkene}]$ source term and $[SA]\cdot CS+ \beta\cdot[SA]^2$ sink term under clean condition. Then we then took data from another period to further evaluate the reliability of the proposed source and sink balance. For spring period from 20th March to 20th May 2019 (Fig. S7 (b)), there is also a good linear correlation (R^2=0.98) when source term is smaller than 6.0×10^{33} $(cm^{-3})^3$ with k_{app} of 1.5×10^{-30} cm^6s^{-2}. Although the fitted k_{app} values deviate beween these two periods, they are in the same order of magnitude. During spring period, apart from the above-mentioned six alkenes, biogenic emitted monoterpenes, which cannot be measured by our instrument and therefore are not included in the source term, start to have a bigger contribution, which likely leads to the deviation of k_{app}. Besides, the yield of sCI and the rate constant between sCI and SO_2 are to some extent temperature-dependent (Berndt et al., 2014), which may further explain at least a part of the difference of k_{app} between winter and spring observations.

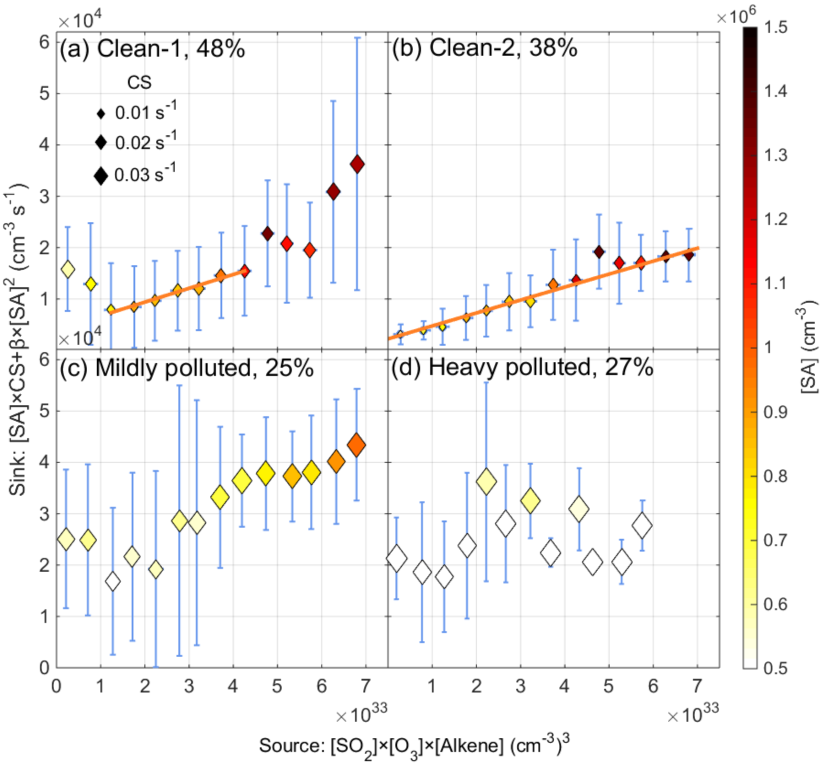

Fig. 5 Correlation between the source term ([SO$_2$]·[O$_3$]·[Alkene]) and sink term ([SA]·CS+β·[SA]^2) of SA under PSS assumption during nighttime (20:00-04:00) from 18th January to 16th March, 2019 for (a) Clean-1 condition, (b) Clean-2 condition, (c) mildly polluted condition and (d) heavy polluted condition. Note that the data points are mean values of corresponding bin ranges instead of the original, high time resolution data (Fig. S5). The error bars are the standard deviation of all data points in each bin.

Under mildly polluted conditions (Fig 5 (c)), the source and sink term also have a good linear correlation when source value exceeds 2.5×10^{33} (cm^{-3})^3, while under heavy polluted conditions, the [SO$_2$]·[O$_3$]·[Alkene] source term and [SA]·CS+β·[SA]^2 sink term do not show a strong correlation (Fig. 5 (d)). Most likely, this suggests that the source term cannot fully represent the actual SA source for heavy polluted conditions. For instance, there are likely additional sources of SA, such as direct emission from diesel vehicles, oil refineries, SA plants, and any other factories that use coal as heating or power supply (Srivastava et al., 2004;Arnold et al., 2006;Ahn et al., 2011;Roy et al., 2014;Sarnela et al., 2015;Godunov et al., 2017). Another possible cause for the correlation deviation under polluted condition, and to some extent also mildly polluted condition, is that the distribution of alkenes may not be constant for measurements classified into the same pollution level, that is, the k_{app} is not constant. At very clean nights when alkenes sources are considered more local and stable, dramatic changes in alkene distribution are not expected. Moreover, our instrument is only capable of measuring a limited amount of alkene species and the fitted parameter k_{app} might be overestimated.

It should be pointed out that we are not able to further deconvolute the contribution of OH radical and sCI based on the ambient observation. A well-tuned box model is a useful tool to resolve it and verify the role of the ozonolysis of alkenes on the nighttime SA formation. However, such a modeling work is not included in our study, as the lacking of a complete VOC datasets in our measurement and the largely uncertain yields of sCI from the ozonolysis of various alkenes have caused challenges in ensuring the precision of the box-model.

4.4 Atmospheric Implication: Contribution of Nighttime Sulfuric Acid to Sub-3nm Particles

We show that the ozonolysis of alkenes is the major source for the considerable amount of SA that exists at night, at least under unpolluted conditions. And it is found that increasing SA concentration coincided with increasing number concentration of sub-3nm particles (Fig. 6), suggesting that SA had a strong enhancement in the formation of newly formed particles, which is consistent with previous study (Cai et al., 2017). Different from SA, there was a negative correlation between the concentration of highly oxygenated organic molecules (HOMs) and $N_{Sub\text{-}3nm}$ for both nighttime and daytime (see Fig. S8 in the supplement), indicating that HOMs were not the main driver for the formation of sub-3nm particles. Then, these elevated SA concentration has the dominant contribution to the formation of sub-3nm particles in the nighttime of winter Beijing. This phenomenon is in contrast with some previous observations in forested areas where oxidation products of biogenic VOCs, especially monoterpene, were the main contributor to the formation of clusters (Eerdekens et al., 2009;Lehtipalo et al., 2011;Kammer et al., 2018;Rose et al., 2018). Both observation (Rose et al., 2018) and laboratory experiment (Lehtipalo et al., 2018) have shown that HOM dimers with extremely low volatility play a key role in the initial formation of clusters; however at our site in urban Beijing, high level of NO_x inhibited the production of HOM dimers and most HOMs are monomers, which have minor importance to the formation of sub-3nm particles. Nighttime sub-3nm particles has also been observed at suburban site (Kecorius et al., 2015) or areas which are strongly influenced by coastal air masses (Yu et al., 2014;Salimi et al., 2017), but the underlying mechanism are still unclear.

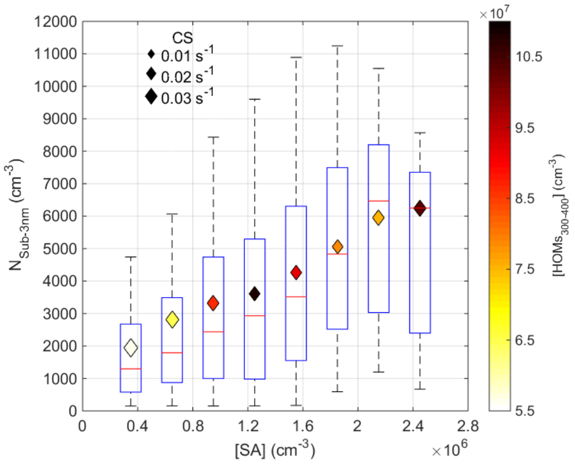

Fig. 6 Correlation between $N_{Sub\text{-}3nm}$ and SA concentration during nighttime (20:00-04:00) from 18th January to 16th March 2019. The binned diamonds are colored by number concentration of HOMs (m/Q = 300 - 400 Th) and the size is related to CS. The red line is the median value, the bottom and the top blue lines are the 25 and 75 percentiles, and the whisker ranges cover the ± 2.7σ of those data in each bin.

5. Conclusions

Continuous SA measurement was conducted during the heating-supply period in urban Beijing. Frequent nighttime SA events were found and accounted for about 32 % of the total measurement nights. Most nighttime SA events were observed under unpolluted conditions and associated with a distinct drop of CS. We show that the SA source corresponding to the product of O_3, alkenes and SO_2 concentrations correlates well with the SA sink for clean conditions, and to some extent also for mildly polluted conditions. Therefore, we suggest that nighttime SA formation under these conditions can be largely attributed to the ozonolysis of alkenes which leads to the production of OH radicals as well as sCI that are able to act as oxidants for SO_2. However, further deconvolution of the contribution of OH radicals, sCI and each possible alkene precursor was not possible within this study due to the inability to directly measure OH, sCI and the entire range of alkene precursors. It should also be pointed out that, under polluted conditions, there were very likely additional SA sources other than the ozonolysis of alkenes, such as direct emission from diesel vehicles, oil refineries and SA plants. Furthermore, we showed that these elevated SA had a dominant contribution to the formation of sub-3nm particles in the nighttime of winter Beijing.

Acknowledgements

This project has received funding from the National Natural Science Foundation of China (41877306), the ERC advanced grant No. 742206, the European Union’s Horizon 2020 research and innovation program under grant agreement No. 654109, the Academy of Finland Center of Excellence Project No. 27204. Kaspar R. Daellenbach acknowledges the support by the SNF mobility grant P2EZP2_181599.

References

Aalto, P., Hämeri, K., Becker, E., Weber, R., Salm, J., Mäkelä, J. M., Hoell, C., O’dowd, C. D., Hansson, H.-C., Väkevä, M., Koponen, I. K., Buzorius, G., and Kulmala, M.: Physical characterization of aerosol particles during nucleation events, Tellus B: Chemical and Physical Meteorology, 53, 344-358, 10.3402/tellusb.v53i4.17127, 2001.

Ahn, J. Y., Okerlund, R., Fry, A., and Eddings, E. G.: Sulfur trioxide formation during oxy-coal combustion, International Journal of Greenhouse Gas Control, 5, S127-S135, 10.1016/j.ijggc.2011.05.009, 2011.

Almeida, J., Schobesberger, S., Kuerten, A., Ortega, I. K., Kupiainen-Maatta, O., Praplan, A. P., Adamov, A., Amorim, A., Bianchi, F., Breitenlechner, M., David, A., Dommen, J., Donahue, N. M., Downard, A., Dunne, E., Duplissy, J., Ehrhart, S., Flagan, R. C., Franchin, A., Guida, R., Hakala, J., Hansel, A., Heinritzi, M., Henschel, H., Jokinen, T., Junninen, H., Kajos, M., Kangasluoma, J., Keskinen, H., Kupc, A., Kurten, T., Kvashin, A. N., Laaksonen, A., Lehtipalo, K., Leiminger, M., Leppa, J., Loukonen, V., Makhmutov, V., Mathot, S., McGrath, M. J., Nieminen, T., Olenius, T., Onnela, A., Petaja, T., Riccobono, F., Riipinen, I., Rissanen, M., Rondo, L., Ruuskanen, T., Santos, F. D., Sarnela, N., Schallhart, S., Schnitzhofer, R., Seinfeld, J. H., Simon, M., Sipila, M., Stozhkov, Y., Stratmann, F., Tome, A., Troestl, J., Tsagkogeorgas, G., Vaattovaara, P., Viisanen, Y., Virtanen, A., Vrtala, A., Wagner, P. E., Weingartner, E., Wex, H., Williamson, C., Wimmer, D., Ye, P., Yli-Juuti, T., Carslaw, K. S., Kulmala, M., Curtius, J., Baltensperger, U., Worsnop, D. R., Vehkamaki, H., and Kirkby, J.: Molecular understanding of sulphuric acid-amine particle nucleation in the atmosphere, Nature, 502, 359-+, 10.1038/nature12663, 2013.

Armendariz, A. J., and Leith, D.: Concentration measurement and counting efficiency for the aerodynamic particle sizer 3320, Journal of Aerosol Science, 33, 133-148, https://doi.org/10.1016/S0021-8502(01)00152-5, 2002.

Arnold, F., Pirjola, L., Aufmhoff, H., Schuck, T., Lahde, T., and Hameri, K.: First gaseous sulfuric acid measurements in automobile exhaust: Implications for volatile nanoparticle formation, Atmospheric Environment, 40, 7097-7105, 10.1016/j.atmosenv.2006.06.038, 2006.

Aschmann, S. M.: OH Radical Production from the Gas-Phase Reaction of O3 with a Series of Alkenes under Atmospheric Conditions, Environmental Science and Technology, 27, 1357-1363, 1993.

Aschmann, S. M., Tuazon, E. C., Arey, J., and Atkinson, R.: Products of the Gas-Phase Reaction of O3 with Cyclohexene, The Journal of Physical Chemistry A, 107, 2247-2255, 10.1021/jp022122e, 2003.

Atkinson, R., Aschmann, S. M., Arey, J., and Shorees, B.: Formation of OH radicals in the gas phase reactions of O3 with a series of terpenes, Journal of Geophysical Research: Atmospheres, 97, 6065-6073, 10.1029/92JD00062, 1992.

Atkinson, R., Baulch, D. L., Cox, R. A., Crowley, J. N., Hampson, R. F., Hynes, R. G., Jenkin, M. E., Rossi, M. J., and Troe, J.: Evaluated kinetic and photochemical data for atmospheric chemistry: Volume II - gas phase reactions of organic species, Atmospheric Chemistry and Physics, 6, 3625-4055, 10.5194/acp-6-3625-2006, 2006.

Berndt, T., Böge, O., and Stratmann, F.: Gas-phase ozonolysis of α-pinene: gaseous products and particle formation, Atmospheric Environment, 37, 3933-3945, https://doi.org/10.1016/S1352-2310(03)00501-6, 2003.

Berndt, T., Jokinen, T., Sipila, M., Mauldin, R. L., III, Herrmann, H., Stratmann, F., Junninen, H., and Kulmala, M.: H2SO4 formation from the gas-phase reaction of stabilized Criegee Intermediates with SO2: Influence of water vapour content and temperature, Atmospheric Environment, 89, 603-612, 10.1016/j.atmosenv.2014.02.062, 2014.

Birmili, W., Berresheim, H., Plass-Dulmer, C., Elste, T., Gilge, S., Wiedensohler, A., and Uhrner, U.: The Hohenpeissenberg aerosol formation experiment (HAFEX): a long-term study including size-resolved aerosol, H2SO4, OH, and monoterpenes measurements, Atmospheric Chemistry and Physics, 3, 361-376, 10.5194/acp-3-361-2003, 2003.

Boy, M., Karl, T., Turnipseed, A., Mauldin, R. L., Kosciuch, E., Greenberg, J., Rathbone, J., Smith, J., Held, A., Barsanti, K., Wehner, B., Bauer, S., Wiedensohler, A., Bonn, B., Kulmala, M., and Guenther, A.: New particle formation in the front range of the colorado rocky mountains, Atmospheric Chemistry and Physics, 8, 1577-1590, 10.5194/acp-8-1577-2008, 2008.

Cai, R., Yang, D., Fu, Y., Wang, X., Li, X., Ma, Y., Hao, J., Zheng, J., and Jiang, J.: Aerosol surface area concentration: a governing factor in new particle formation in Beijing, Atmospheric Chemistry and Physics, 17, 12327-12340, 10.5194/acp-17-12327-2017, 2017.

Chew, A. A., and Atkinson, R.: OH radical formation yields from the gas-phase reactions of O3 with alkenes and monoterpenes, Journal of Geophysical Research: Atmospheres, 101, 28649-28653, 10.1029/96JD02722, 1996.

Dada, L., Ylivinkka, I., Baalbaki, R., Li, C., Guo, Y., Yan, C., Yao, L., Sarnela, N., Jokinen, T., Daellenbach, K. R., Yin, R., Deng, C., Chu, B., Nieminen, T., Kontkanen, J., Stolzenburg, D., Sipilä, M., Hussein, T., Paasonen, P., Bianchi, F., Salma, I., Weidinger, T., Pikridas, M., Sciare, J., Jiang, J., Liu, Y., Petäjä, T., Kerminen, V. M., and Kulmala, M.: Sources and sinks driving sulphuric acid concentrations in contrasting environments: implications on proxy calculations, Atmos. Chem. Phys. Discuss., 2020, 1-24, 10.5194/acp-2020-155, 2020.

Eerdekens, G., Yassaa, N., Sinha, V., Aalto, P. P., Aufmhoff, H., Arnold, F., Fiedler, V., Kulmala, M., and Williams, J.: VOC measurements within a boreal forest during spring 2005: on the occurrence of elevated monoterpene concentrations during night time intense particle concentration events, Atmospheric Chemistry and Physics, 9, 8331-8350, 10.5194/acp-9-8331-2009, 2009.

Eisele, F. L., Lovejoy, E. R., Kosciuch, E., Moore, K. F., Mauldin, R. L., Smith, J. N., McMurry, P. H., and Iida, K.: Negative atmospheric ions and their potential role in ion-induced nucleation, Journal of Geophysical Research-Atmospheres, 111, 10.1029/2005jd006568, 2006.

Erupe, M. E., Benson, D. R., Li, J., Young, L.-H., Verheggen, B., Al-Refai, M., Tahboub, O., Cunningham, V., Frimpong, F., Viggiano, A. A., and Lee, S.-H.: Correlation of aerosol nucleation rate with sulfuric acid and ammonia in Kent, Ohio: An atmospheric observation, Journal of Geophysical Research-Atmospheres, 115, 10.1029/2010jd013942, 2010.

Fenske, J. D., Hasson, A. S., Ho, A. W., and Paulson, S. E.: Measurement of Absolute Unimolecular and Bimolecular Rate Constants for CH3CHOO Generated by the trans-2-Butene Reaction with Ozone in the Gas Phase, The Journal of Physical Chemistry A, 104, 9921-9932, 10.1021/jp0016636, 2000.

Fiedler, V., Dal Maso, M., Boy, M., Aufmhoff, H., Hoffmann, J., Schuck, T., Birmili, W., Hanke, M., Uecker, J., Arnold, F., and Kulmala, M.: The contribution of sulphuric acid to atmospheric particle formation and growth: a comparison between boundary layers in Northern and Central Europe, Atmospheric Chemistry and Physics, 5, 1773-1785, 10.5194/acp-5-1773-2005, 2005.

Gao, W., Tan, G., Hong, Y., Li, M., Nian, H., Guo, C., Huang, Z., Fu, Z., Dong, J., Xu, X., Cheng, P., and Zhou, Z.: Development of portable single photon ionization time-of-flight mass spectrometer combined with membrane inlet, International Journal of Mass Spectrometry, 334, 8-12, 10.1016/j.ijms.2012.09.003, 2013.

Godunov, E. B., Kuznetsova, I. A., and Klevleev, V. M.: Comprehensive Utilization of Spent Sulfuric Acid from Petrochemical Industries and Chemical Current Sources, Chemical and Petroleum Engineering, 53, 531-533, 10.1007/s10556-017-0376-9, 2017.

Hasson, A. S., Orzechowska, G., and Paulson, S. E.: Production of stabilized Criegee intermediates and peroxides in the gas phase ozonolysis of alkenes 1. Ethene, trans-2-butene, and 2,3-dimethyl-2-butene, Journal of Geophysical Research-Atmospheres, 106, 34131-34142, 10.1029/2001jd000597, 2001.

Hatakeyama, S., Kobayashi, H., and Akimoto, H.: Gas-phase oxidation of sulfur dioxide in the ozone-olefin reactions, The Journal of Physical Chemistry, 88, 4736-4739, 10.1021/j150664a058, 1984.

Huang, H.-L., Chao, W., and Lin, J. J.-M.: Kinetics of a Criegee intermediate that would survive high humidity and may oxidize atmospheric SO2, Proceedings of the National Academy of Sciences of the United States of America, 112, 10857-10862, 10.1073/pnas.1513149112, 2015.

Iida, K., Stolzenburg, M. R., McMurry, P. H., and Smith, J. N.: Estimating nanoparticle growth rates from size-dependent charged fractions: Analysis of new particle formation events in Mexico City, Journal of Geophysical Research-Atmospheres, 113, 10.1029/2007jd009260, 2008.

Jokinen, T., Sipila, M., Junninen, H., Ehn, M., Lonn, G., Hakala, J., Petaja, T., Mauldin, R. L., III, Kulmala, M., and Worsnop, D. R.: Atmospheric sulphuric acid and neutral cluster measurements using CI-APi-TOF, Atmospheric Chemistry and Physics, 12, 4117-4125, 10.5194/acp-12-4117-2012, 2012.

Jokinen, T., Sipila, M., Kontkanen, J., Vakkari, V., Tisler, P., Duplissy, E. M., Junninen, H., Kangasluoma, J., Manninen, H. E., Petaja, T., Kulmala, M., Worsnop, D. R., Kirkby, J., Virkkula, A., and Kerminen, V. M.: Ion-induced sulfuric acid-ammonia nucleation drives particle formation in coastal Antarctica, Science Advances, 4, 10.1126/sciadv.aat9744, 2018.

Junninen, H., Hulkkonen, M., Riipinen, I., Nieminen, T., Hirsikko, A., Suni, T., Boy, M., Lee, S.-H., Vana, M., Tammet, H., Kerminen, V.-M., and Kulmala, M.: Observations on nocturnal growth of atmospheric clusters, Tellus Series B-Chemical and Physical Meteorology, 60, 365-371, 10.1111/j.1600-0889.2008.00356.x, 2008.

Kammer, J., Perraudin, E., Flaud, P. M., Lamaud, E., Bonnefond, J. M., and Villenave, E.: Observation of nighttime new particle formation over the French Landes forest, Science of the Total Environment, 621, 1084-1092, 10.1016/j.scitotenv.2017.10.118, 2018.

Kecorius, S., Zhang, S., Wang, Z., Groess, J., Ma, N., Wu, Z., Ran, L., Hu, M., Wang, P., Ulevicius, V., and Wiedensohler, A.: NOCTURNAL AEROSOL PARTICLE FORMATION IN THE NORTH CHINA PLAIN, Lithuanian Journal of Physics, 55, 44-53, 2015.

Kirkby, J., Curtius, J., Almeida, J., Dunne, E., Duplissy, J., Ehrhart, S., Franchin, A., Gagne, S., Ickes, L., Kuerten, A., Kupc, A., Metzger, A., Riccobono, F., Rondo, L., Schobesberger, S., Tsagkogeorgas, G., Wimmer, D., Amorim, A., Bianchi, F., Breitenlechner, M., David, A., Dommen, J., Downard, A., Ehn, M., Flagan, R. C., Haider, S., Hansel, A., Hauser, D., Jud, W., Junninen, H., Kreissl, F., Kvashin, A., Laaksonen, A., Lehtipalo, K., Lima, J., Lovejoy, E. R., Makhmutov, V., Mathot, S., Mikkila, J., Minginette, P., Mogo, S., Nieminen, T., Onnela, A., Pereira, P., Petaja, T., Schnitzhofer, R., Seinfeld, J. H., Sipila, M., Stozhkov, Y., Stratmann, F., Tome, A., Vanhanen, J., Viisanen, Y., Vrtala, A., Wagner, P. E., Walther, H., Weingartner, E., Wex, H., Winkler, P. M., Carslaw, K. S., Worsnop, D. R., Baltensperger, U., and Kulmala, M.: Role of sulphuric acid, ammonia and galactic cosmic rays in atmospheric aerosol nucleation, Nature, 476, 429-U477, 10.1038/nature10343, 2011.

Kotzias, D., Fytianos, K., and Geiss, F.: Reaction of monoterpenes with ozone, sulphur dioxide and nitrogen dioxide—gas-phase oxidation of SO2 and formation of sulphuric acid, Atmospheric Environment. Part A. General Topics, 24, 2127-2132, https://doi.org/10.1016/0960-1686(90)90246-J, 1990.

Kuerten, A., Jokinen, T., Simon, M., Sipila, M., Sarnela, N., Junninen, H., Adamov, A., Almeida, J., Amorim, A., Bianchi, F., Breitenlechner, M., Dommen, J., Donahue, N. M., Duplissy, J., Ehrhart, S., Flagan, R. C., Franchin, A., Hakala, J., Hansel, A., Heinritzi, M., Hutterli, M., Kangasluoma, J., Kirkby, J., Laaksonen, A., Lehtipalo, K., Leiminger, M., Makhmutov, V., Mathot, S., Onnela, A., Petaja, T., Praplan, A. P., Riccobono, F., Rissanen, M. P., Rondo, L., Schobesberger, S., Seinfeld, J. H., Steiner, G., Tome, A., Troestl, J., Winkler, P. M., Williamson, C., Wimmer, D., Ye, P., Baltensperger, U., Carslaw, K. S., Kulmala, M., Worsnop, D. R., and Curtius, J.: Neutral molecular cluster formation of sulfuric acid-dimethylamine observed in real time under atmospheric conditions, Proceedings of the National Academy of Sciences of the United States of America, 111, 15019-15024, 10.1073/pnas.1404853111, 2014.

Kuerten, A., Bergen, A., Heinritzi, M., Leiminger, M., Lorenz, V., Piel, F., Simon, M., Sitals, R., Wagner, A. C., and Curtius, J.: Observation of new particle formation and measurement of sulfuric acid, ammonia, amines and highly oxidized organic molecules at a rural site in central Germany, Atmospheric Chemistry and Physics, 16, 12793-12813, 10.5194/acp-16-12793-

2016, 2016.

Kulmala, M., Maso, M. D., Mäkelä, J. M., Pirjola, L., Väkevä, M., Aalto, P., Miikkulainen, P., Hämeri, K., and O'dowd, C. D.: On the formation, growth and composition of nucleation mode particles, Tellus B: Chemical and Physical Meteorology, 53, 479-490, 10.3402/tellusb.v53i4.16622, 2001.

Kulmala, M., Lehtinen, K. E. J., and Laaksonen, A.: Cluster activation theory as an explanation of the linear dependence between formation rate of 3nm particles and sulphuric acid concentration, Atmospheric Chemistry and Physics, 6, 787-793, 10.5194/acp-6-787-2006, 2006.

Kulmala, M., Kontkanen, J., Junninen, H., Lehtipalo, K., Manninen, H. E., Nieminen, T., Petäjä, T., Sipilä, M., Schobesberger, S., Rantala, P., Franchin, A., Jokinen, T., Järvinen, E., Äijälä, M., Kangasluoma, J., Hakala, J., Aalto, P. P., Paasonen, P., Mikkilä, J., Vanhanen, J., Aalto, J., Hakola, H., Makkonen, U., Ruuskanen, T., Mauldin, R. L., Duplissy, J., Vehkamäki, H., Bäck, J., Kortelainen, A., Riipinen, I., Kurtén, T., Johnston, M. V., Smith, J. N., Ehn, M., Mentel, T. F., Lehtinen, K. E. J., Laaksonen, A., Kerminen, V.-M., and Worsnop, D. R.: Direct Observations of Atmospheric Aerosol Nucleation, Science, 339, 943, 10.1126/science.1227385, 2013.

Kurten, A., Rondo, L., Ehrhart, S., and Curtius, J.: Calibration of a Chemical Ionization Mass Spectrometer for the Measurement of Gaseous Sulfuric Acid, Journal of Physical Chemistry A, 116, 6375-6386, 10.1021/jp212123n, 2012.

Lee, S. H., Gordon, H., Yu, H., Lehtipalo, K., Haley, R., Li, Y. X., and Zhang, R. Y.: New Particle Formation in the Atmosphere: From Molecular Clusters to Global Climate, Journal of Geophysical Research-Atmospheres, 124, 7098-7146, 10.1029/2018jd029356, 2019.

Lehtipalo, K., Sipila, M., Junninen, H., Ehn, M., Berndt, T., Kajos, M. K., Worsnop, D. R., Petaja, T., and Kulmala, M.: Observations of Nano-CN in the Nocturnal Boreal Forest, Aerosol Science and Technology, 45, 499-509, 10.1080/02786826.2010.547537, 2011.

Lehtipalo, K., Yan, C., Dada, L., Bianchi, F., Xiao, M., Wagner, R., Stolzenburg, D., Ahonen, L. R., Amorim, A., Baccarini, A., Bauer, P. S., Baumgartner, B., Bergen, A., Bernhammer, A.-K., Breitenlechner, M., Brilke, S., Buchholz, A., Mazon, S. B., Chen, D., Chen, X., Dias, A., Dommen, J., Draper, D. C., Duplissy, J., Ehn, M., Finkenzeller, H., Fischer, L., Frege, C., Fuchs, C., Garmash, O., Gordon, H., Hakala, J., He, X., Heikkinen, L., Heinritzi, M., Helm, J. C., Hofbauer, V., Hoyle, C. R., Jokinen, T., Kangasluoma, J., Kerminen, V.-M., Kim, C., Kirkby, J., Kontkanen, J., Kuerten, A., Lawler, M. J., Mai, H., Mathot, S., Mauldin, R. L., III, Molteni, U., Nichman, L., Nie, W., Nieminen, T., Ojdanic, A., Onnela, A., Passananti, M., Petaja, T., Piel, F., Pospisilova, V., Quelever, L. L. J., Rissanen, M. P., Rose, C., Sarnela, N., Schallhart, S., Schuchmann, S., Sengupta, K., Simon, M., Sipila, M., Tauber, C., Tome, A., Trostl, J., Vaisanen, O., Vogel, A. L., Volkamer, R., Wagner, A. C., Wang, M., Weitz, L., Wimmer, D., Ye, P., Ylisirnio, A., Zha, Q., Carslaw, K. S., Curtius, J., Donahue, N. M., Flagan, R. C., Hansel, A., Riipinen, I., Virtanen, A., Winkler, P. M., Baltensperger, U., Kulmala, M., and Worsnop, D. R.: Multicomponent new particle formation from sulfuric acid, ammonia, and biogenic vapors, Science Advances, 4, 10.1126/sciadv.aau5363, 2018.

Lu, Y., Yan, C., Fu, Y., Chen, Y., Liu, Y., Yang, G., Wang, Y., Bianchi, F., Chu, B., Zhou, Y., Yin, R., Baalbaki, R., Garmash, O., Deng, C., Wang, W., Liu, Y., Petaja, T., Kerminen, V.-M., Jiang, J., Kulmala, M., and Wang, L.: A proxy for atmospheric daytime gaseous sulfuric acid concentration in urban Beijing, Atmospheric Chemistry and Physics, 19, 1971-1983, 10.5194/acp-19-1971-2019, 2019.

Malkin, T. L., Goddard, A., Heard, D. E., and Seakins, P. W.: Measurements of OH and HO2 yields from the gas phase ozonolysis of isoprene, Atmospheric Chemistry and Physics, 10, 1441-1459, 10.5194/acp-10-1441-2010, 2010.

Mauldin, R. L., Eisele, F. L., Tanner, D. J., Kosciuch, E., Shetter, R., Lefer, B., Hall, S. R., Nowak, J. B., Buhr, M., Chen, G., Wang, P., and Davis, D.: Measurements of OH, H2SO4, and MSA at the South Pole during ISCAT, Geophysical Research Letters, 28, 3629-3632, 10.1029/2000gl012711, 2001.

Mauldin, R. L., III, Berndt, T., Sipilae, M., Paasonen, P., Petaja, T., Kim, S., Kurten, T., Stratmann, F., Kerminen, V. M., and Kulmala, M.: A new atmospherically relevant oxidant of sulphur dioxide, Nature, 488, 193-196, 10.1038/nature11278, 2012.

Mazon, S. B., Kontkanen, J., Manninen, H. E., Nieminen, T., Kerminen, V.-M., and Kulmala, M.: A long-term comparison of nighttime cluster events and daytime ion formation in a boreal forest, Boreal Environment Research, 21, 242-261, 2016.

McMurry, P. H., Fink, M., Sakurai, H., Stolzenburg, M. R., Mauldin, R. L., Smith, J., Eisele, F., Moore, K., Sjostedt, S., Tanner, D., Huey, L. G., Nowak, J. B., Edgerton, E., and Voisin, D.: A criterion for new particle formation in the sulfur-rich Atlanta atmosphere, Journal of Geophysical Research-Atmospheres, 110, 10.1029/2005jd005901, 2005.

Myllys, N., Chee, S., Olenius, T., Lawler, M., and Smith, J.: Molecular-Level Understanding of Synergistic Effects in Sulfuric Acid-Amine-Ammonia Mixed Clusters, Journal of Physical Chemistry A, 123, 2420-2425, 10.1021/acs.jpca.9b00909, 2019.

Neeb, P., Sauer, F., Horie, O., and Moortgat, G. K.: Formation of hydroxymethyl hydroperoxide and formic acid in alkene ozonolysis in the presence of water vapour, Atmospheric Environment, 31, 1417-1423, https://doi.org/10.1016/S1352-2310(96)00322-6, 1997.

Newland, M. J., Rickard, A. R., Alam, M. S., Vereecken, L., Munoz, A., Rodenas, M., and Bloss, W. J.: Kinetics of stabilised Criegee intermediates derived from alkene ozonolysis: reactions with SO2, H2O and decomposition under boundary layer conditions, Physical Chemistry Chemical Physics, 17, 4076-4088, 10.1039/c4cp04186k, 2015a.

Newland, M. J., Rickard, A. R., Vereecken, L., Munoz, A., Rodenas, M., and Bloss, W. J.: Atmospheric isoprene ozonolysis: impacts of stabilised Criegee intermediate reactions with SO2, H2O and dimethyl sulfide, Atmospheric Chemistry and Physics, 15, 9521-9536, 10.5194/acp-15-9521-2015, 2015b.

Nguyen, T. L., Peeters, J., and Vereecken, L.: Theoretical study of the gas-phase ozonolysis of beta-pinene (C10H16), Physical Chemistry Chemical Physics, 11, 5643-5656, 10.1039/b822984h, 2009.

Paasonen, P., Sihto, S.-L., Nieminen, T., Vuollekoski, H., Riipinen, I., Plass-Dulmer, C., Berresheim, H., Birmili, W., and Kulmala, M.: Connection between new particle formation and sulphuric acid at Hohenpeissenberg (Germany) including the influence of organic compounds, Boreal Environment Research, 14, 616-629, 2009.

Paasonen, P., Nieminen, T., Asmi, E., Manninen, H. E., Petaja, T., Plass-Duelmer, C., Flentje, H., Birmili, W., Wiedensohler, A., Horrak, U., Metzger, A., Hamed, A., Laaksonen, A., Facchini, M. C., Kerminen, V. M., and Kulmala, M.: On the roles of sulphuric acid and low-volatility organic vapours in the initial steps of atmospheric new particle formation, Atmospheric Chemistry and Physics, 10, 11223-11242, 10.5194/acp-10-11223-2010, 2010.

Riccobono, F., Schobesberger, S., Scott, C. E., Dommen, J., Ortega, I. K., Rondo, L., Almeida, J., Amorim, A., Bianchi, F., Breitenlechner, M., David, A., Downard, A., Dunne, E. M., Duplissy, J., Ehrhart, S., Flagan, R. C., Franchin, A., Hansel, A., Junninen, H., Kajos, M., Keskinen, H., Kupc, A., Kuerten, A., Kvashin, A. N., Laaksonen, A., Lehtipalo, K., Makhmutov, V., Mathot, S., Nieminen, T., Onnela, A., Petaja, T., Praplan, A. P., Santos, F. D., Schallhart, S., Seinfeld, J. H., Sipila, M., Spracklen, D. V., Stozhkov, Y., Stratmann, F., Tome, A., Tsagkogeorgas, G., Vaattovaara, P., Viisanen, Y., Vrtala, A., Wagner, P. E., Weingartner, E., Wex, H., Wimmer, D., Carslaw, K. S., Curtius, J., Donahue, N. M., Kirkby, J., Kulmala, M., Worsnop, D. R., and Baltensperger, U.: Oxidation Products of Biogenic Emissions Contribute to Nucleation of Atmospheric Particles, Science, 344, 717-721, 10.1126/science.1243527, 2014.

Rickard, A. R., Johnson, D., McGill, C. D., and Marston, G.: OH Yields in the Gas-Phase Reactions of Ozone with Alkenes, The Journal of Physical Chemistry A, 103, 7656-7664, 10.1021/jp9916992, 1999.

Riipinen, I., Sihto, S. L., Kulmala, M., Arnold, F., Dal Maso, M., Birmili, W., Saarnio, K., Teinila, K., Kerminen, V. M., Laaksonen, A., and Lehtinen, K. E. J.: Connections between atmospheric sulphuric acid and new particle formation during QUEST III-IV campaigns in Heidelberg and Hyyti, Atmospheric Chemistry and Physics, 7, 1899-1914, 10.5194/acp-7-1899-2007, 2007.

Rose, C., Zha, Q., Dada, L., Yan, C., Lehtipalo, K., Junninen, H., Mazon, S. B., Jokinen, T., Sarnela, N., Sipila, M., Petaja, T., Kerminen, V.-M., Bianchi, F., and Kulmala, M.: Observations of biogenic ion-induced cluster formation in the atmosphere, Science Advances, 4, 10.1126/sciadv.aar5218, 2018.

Roy, B., Chen, L., and Bhattacharya, S.: Nitrogen Oxides, Sulfur Trioxide, and Mercury Emissions during Oxyfuel Fluidized Bed Combustion of Victorian Brown Coal, Environmental Science & Technology, 48, 14844-14850, 10.1021/es504667r, 2014.

Salimi, F., Rahman, M. M., Clifford, S., Ristovski, Z., and Morawska, L.: Nocturnal new particle formation events in urban environments, Atmos. Chem. Phys., 17, 521-530, 10.5194/acp-17-521-2017, 2017.

Sarnela, N., Jokinen, T., Nieminen, T., Lehtipalo, K., Junninen, H., Kangasluoma, J., Hakala, J., Taipale, R., Schobesberger, S., Sipila, M., Larnimaa, K., Westerholm, H., Heijari, J., Kerminen, V.-M., Petaja, T., and Kulmala, M.: Sulphuric acid and aerosol particle production in the vicinity of an oil refinery, Atmospheric Environment, 119, 156-166, 10.1016/j.atmosenv.2015.08.033, 2015.

Seinfeld, J. H., and Pandis, S. N.: Atmospheric chemistry and physics: from air pollution to climate change, John Wiley & Sons, 2016.

Siese, M., Becker, K. H., Brockmann, K. J., Geiger, H., Hofzumahaus, A., Holland, F., Mihelcic, D., and Wirtz, K.: Direct Measurement of OH Radicals from Ozonolysis of Selected Alkenes: A EUPHORE Simulation Chamber Study, Environmental Science & Technology, 35, 4660-4667, 10.1021/es010150p, 2001.

Sipila, M., Jokinen, T., Berndt, T., Richters, S., Makkonen, R., Donahue, N. M., Mauldin, R. L., III, Kurten, T., Paasonen, P., Sarnela, N., Ehn, M., Junninen, H., Rissanen, M. P., Thornton, J., Stratmann, F., Herrmann, H., Worsnop, D. R., Kulmala, M., Kerminen, V. M., and Petaja, T.: Reactivity of stabilized Criegee intermediates (sCIs) from isoprene and monoterpene ozonolysis toward SO2 and organic acids, Atmospheric Chemistry and Physics, 14, 12143-12153, 10.5194/acp-14-12143-2014, 2014.

Srivastava, R. K., Miller, C. A., Erickson, C., and Jambhekar, R.: Emissions of sulfur trioxide from coal-fired power plants, Journal of the Air & Waste Management Association, 54, 750-762, 10.1080/10473289.2004.10470943, 2004.

Stocker, T. F., Qin, D., Plattner, G.-K., Tignor, M. M., Allen, S. K., Boschung, J., Nauels, A., Xia, Y., Bex, V., and Midgley, P. M.: Climate Change 2013: The physical science basis. contribution of working group I to the fifth assessment report of IPCC the intergovernmental panel on climate change, in, Cambridge University Press, 2014.

Taatjes, C. A., Welz, O., Eskola, A. J., Savee, J. D., Scheer, A. M., Shallcross, D. E., Rotavera, B., Lee, E. P. F., Dyke, J. M., Mok, D. K. W., Osborn, D. L., and Percival, C. J.: Direct Measurements of Conformer-Dependent Reactivity of the Criegee Intermediate CH3CHOO, Science, 340, 177-180, 10.1126/science.1234689, 2013.

Taipale, R., Sarnela, N., Rissanen, M., Junninen, H., Rantala, P., Korhonen, F., Siivola, E., Berndt, T., Kulmala, M., Mauldin, R. L., III, Petaja, T., and Sipila, M.: New instrument for measuring atmospheric concentrations of non-OH oxidants of SO2, Boreal Environment Research, 19, 55-70, 2014.

Vanhanen, J., Mikkila, J., Lehtipalo, K., Sipila, M., Manninen, H. E., Siivola, E., Petaja, T., and Kulmala, M.: Particle Size Magnifier for Nano-CN Detection, Aerosol Science and Technology, 45, 533-542, 10.1080/02786826.2010.547889, 2011.

Vereecken, L., Novelli, A., and Taraborrelli, D.: Unimolecular decay strongly limits the atmospheric impact of Criegee intermediates, Physical Chemistry Chemical Physics, 19, 31599-31612, 10.1039/c7cp05541b, 2017.

Wang, Z. B., Hu, M., Yue, D. L., Zheng, J., Zhang, R. Y., Wiedensohler, A., Wu, Z. J., Nieminen, T., and Boy, M.: Evaluation on the role of sulfuric acid in the mechanisms of new particle formation for Beijing case, Atmospheric Chemistry and Physics, 11, 12663-12671, 10.5194/acp-11-12663-2011, 2011.

Weber, R. J., Marti, J. J., McMurry, P. H., Eisele, F. L., Tanner, D. J., and Jefferson, A.: Measurements of new particle formation and ultrafine particle growth rates at a clean continental site, 102, 4375-4385, 10.1029/96jd03656, 1997.

Weber, R. J., McMurry, P. H., Mauldin, L., Tanner, D. J., Eisele, F. L., Brechtel, F. J., Kreidenweis, S. M., Kok, G. L., Schillawski, R. D., and Baumgardner, D.: A study of new particle formation and growth involving biogenic and trace gas species measured during ACE 1, 103, 16385-16396, 10.1029/97jd02465, 1998.

Weber, R. J., McMurry, P. H., Mauldin III, R. L., Tanner, D. J., Eisele, F. L., Clarke, A. D., and Kapustin, V. N.: New Particle Formation in the Remote Troposphere: A Comparison of Observations at Various Sites, 26, 307-310, 10.1029/1998gl900308, 1999.

Welz, O., Savee, J. D., Osborn, D. L., Vasu, S. S., Percival, C. J., Shallcross, D. E., and Taatjes, C. A.: Direct Kinetic Measurements of Criegee Intermediate (CH2OO) Formed by Reaction of CH2I with O-2, Science, 335, 204-207, 10.1126/science.1213229, 2012.

Welz, O., Eskola, A. J., Sheps, L., Rotavera, B., Savee, J. D., Scheer, A. M., Osborn, D. L., Lowe, D., Booth, A. M., Xiao, P., Khan, M. A. H., Percival, C. J., Shallcross, D. E., and Taatjes, C. A.: Rate Coefficients of C1 and C2 Criegee Intermediate Reactions with Formic and Acetic Acid Near the Collision Limit: Direct Kinetics Measurements and Atmospheric Implications, Angewandte Chemie-International Edition, 53, 4547-4550, 10.1002/anie.201400964, 2014.

Witter, M., Berndt, T., Böge, O., Stratmann, F., and Heintzenberg, J.: Gas-phase ozonolysis: Rate coefficients for a series of terpenes and rate coefficients and OH yields for 2-methyl-2-butene and 2,3-dimethyl-2-butene, International Journal of Chemical Kinetics, 34, 394-403, 10.1002/kin.10063, 2002.

Yao, L., Garmash, O., Bianchi, F., Zheng, J., Yan, C., Kontkanen, J., Junninen, H., Mazon, S. B., Ehn, M., Paasonen, P., Sipila, M., Wang, M. Y., Wang, X. K., Xiao, S., Chen, H. F., Lu, Y. Q., Zhang, B. W., Wang, D. F., Fu, Q. Y., Geng, F. H., Li, L., Wang, H. L., Qiao, L. P., Yang, X., Chen, J. M., Kerminen, V. M., Petaja, T., Worsnop, D. R., Kulmala, M., and Wang, L.: Atmospheric new particle formation from sulfuric acid and amines in a Chinese megacity, Science, 361, 278-+, 10.1126/science.aao4839, 2018.

Yu, H., McGraw, R., and Lee, S.-H.: Effects of amines on formation of sub-3 nm particles and their subsequent growth, Geophysical Research Letters, 39, 10.1029/2011gl050099, 2012.

Yu, H., Hallar, A. G., You, Y., Sedlacek, A., Springston, S., Kanawade, V. P., Lee, Y. N., Wang, J., Kuang, C. G., McGraw, R. L., McCubbin, I., Mikkila, J., and Lee, S. H.: Sub-3nm particles observed at the coastal and continental sites in the United States, Journal of Geophysical Research-Atmospheres, 119, 860-879, 10.1002/2013jd020841, 2014.

Zhang, D., Lei, W. F., and Zhang, R. Y.: Mechanism of OH formation from ozonolysis of isoprene: kinetics and product yields, Chemical Physics Letters, 358, 171-179, 10.1016/s0009-2614(02)00260-9, 2002.

Zhang, D., and Zhang, R.: Ozonolysis of alpha-pinene and beta-pinene: Kinetics and mechanism, Journal of Chemical Physics, 122, 10.1063/1.1862616, 2005.

Supplement of

Formation of Nighttime Sulfuric Acid from the Ozonolysis of Alkenes in Beijing

Yishuo Guo et al.

Correspondence to: Chao Yan (chao.yan@helsinki.fi), Markku Kulmala (markku.kulmala@helsinki.fi)

S1. Conversion of SO_3 to SA

The conversion of SO_3 to SA is based on the following reaction:

$$SO_3 + 2H_2O \xrightarrow{k} H_2SO_4 + H_2O$$

The production rate of SA from SO_3 is:

$$P_{[SA]} = k \cdot [SO_3] \cdot [H_2O]^2$$

where $k=3.9\times10^{-41}\exp(6830.6/T)\ cm^{-6}\ s^{-1}$ (Jayne et al., 1997). During the measurement period, nighttime median concentration of H_2O was $4.97\times10^{16}\ cm^3$, and nighttime median temperature was 276.6 K, then:

$$k \cdot [H_2O]^2 = [3.9 \times 10^{-41} exp(6830.9/276.6)\ \ cm^{-6}\ \ s^{-1}] \times (4.97 \times 10^{16}\ \ cm^3)^2 = 4.88 \times 10^3\ \ s^{-1}$$

The lifetime of SO_3 based on reaction with H_2O is:

$$\tau_{SO_3} = \frac{1}{k \cdot [H_2O]^2} = \frac{1}{4.88 \times 10^3\ \ s^{-1}} = 2.05 \times 10^{-4}\ \ s$$

The lifetime of SO_3 is so short under typical atmospheric conditions, which means that the reaction between SO_3 and H_2O is so fast that all SO_3 will be instantaneously converted to SA. In this case, the oxidation of SO_2 is the rate-limiting step in the formation of SA.

S2. Pseudo-steady-state (PSS) assumption of SA

The net concentration change of gaseous SA is determined by both the source and loss terms, as shown in the following equation:

$$\frac{d[SA]}{dt} = k_{app} \cdot [Alkene] \cdot [O_3] \cdot [SO_2] - [SA] \cdot CS - \beta \cdot [SA]^2$$

where the loss rate and production rate of SA are $L_{SA}=[SA]\cdot CS+\beta\cdot[SA]^2$ and $P_{SA}=L_{SA}+d[SA]/dt$ respectively. We can compare the magnitude of the net concentration change to the overall loss rate. During nighttime (20:00-04:00) from 18th January to 16th March 2019, the median net concentration change of SA is about $181.60\ cm^{-3}s^{-1}$ and the overall SA loss rate at the median SA concentration ($7.52 \times 10^5\ cm^{-3}$) is $1.61 \times 10^4\ cm^{-3}s^{-1}$. As the loss rate (and source rate) is much faster than the net concentration change, the pseudo-steady state (PSS) assumption is valid for SA. Besides, the resolution of the SA data is 5 minutes, and the concentration, net concentration change, loss rate and production rate of SA are listed in Table S4.

S3. Division of pollution level by visibility

Pollution level is kind of an ambiguous concept, and one may judge it by $PM_{2.5}$, while another may judge it by visibility or NO_x. Therefore, we did some efforts to determine the final parameter used to represent pollution level. Fig. S3 shows the correlation of $PM_{2.5}$, CS, RH with visibility. It can be seen that with the increase of visibility, $PM_{2.5}$ decreases monotonically, and RH and CS also have a declining trend. Hence, visibility is a good candidate to represent pollution level. Besides, in the visibility range of 12.0 km to 19.0 km, with the increase of visibility, $PM_{2.5}$ and RH do not vary too much, with CS slightly declining as well, which also implies that visibility is more sensitive than $PM_{2.5}$, RH and CS. Thus, visibility indeed can be used to judge the pollution level for this specific time period of this work.

It also can be found out that the correlation between $PM_{2.5}$ and visibility can be further divided into the following 3 groups: a. visibility < 4.0 km (heavy polluted conditions): visibility and $PM_{2.5}$ have a very good negative linear correlation with R_1 (correlation coefficient) = -1.000, and the decrease rate of visibility is rather fast with the slope of k_1 = -0.0339 $\mu g/m^4$; b. 4.0 km ≤ visibility < 12.0 km (mildly polluted conditions): visibility and $PM_{2.5}$ also have a negative linear correlation with R_2 = -0.9688, but the decrease rate of visibility with $PM_{2.5}$ reduces to k_2 = -0.0084 $\mu g/m^4$; c. visibility ≥ 12.0 km (clean conditions): $PM_{2.5}$ stays constant with varying visibility values, which means that when $PM_{2.5}$ is smaller than 40 $\mu g/m^3$ during heating supply winter period, visibility will be more likely influenced by other factors. In total, data points under the clean conditions mentioned above take up 47.91% of all data points.

Figures

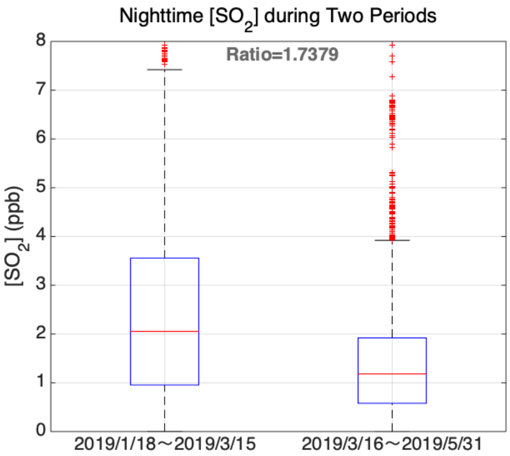

Fig. S1 Boxplot for SO_2 mixing ratio during nighttime (20:00-04:00) in winter-heating-supply period (from 18th January to 15th March 2019) and non-heating-supply period (from 16th March 2019 to 31st May 2019). The middle line in the box is the median, the bottom and the top are the 25 and 75 percentiles, the whisker ranges cover the ± 2.7σ of data in each group, and the red points are the outliers. The dark gray value on the top is the ratio between median SO_2 values of two periods.

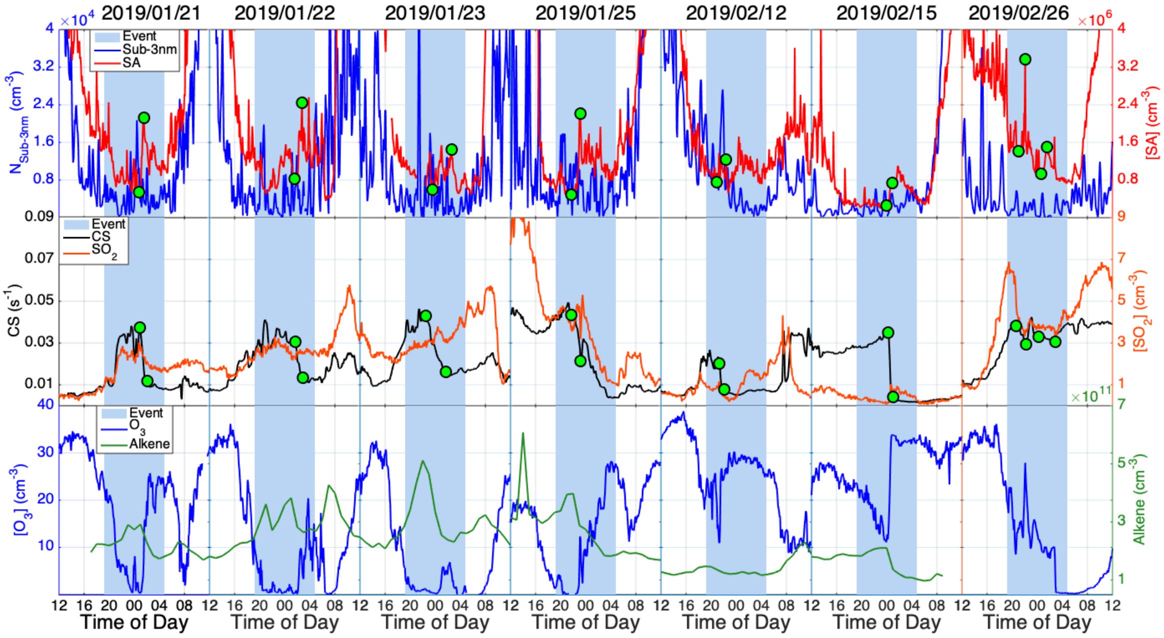

Fig. S2 Daily time-series of different parameters on nighttime SA event days when SA cases occurred under SO_2 increase condition. The first row: $N_{sub-3nm}$ and SA concentration, the second row: CS and SO_2 concentration, and the third row: concentration of O_3 and alkenes. The increase starting points and maximum value points of SA concentration as well as the corresponding SO_2 concentration at the same moments are marked by cyan dots.

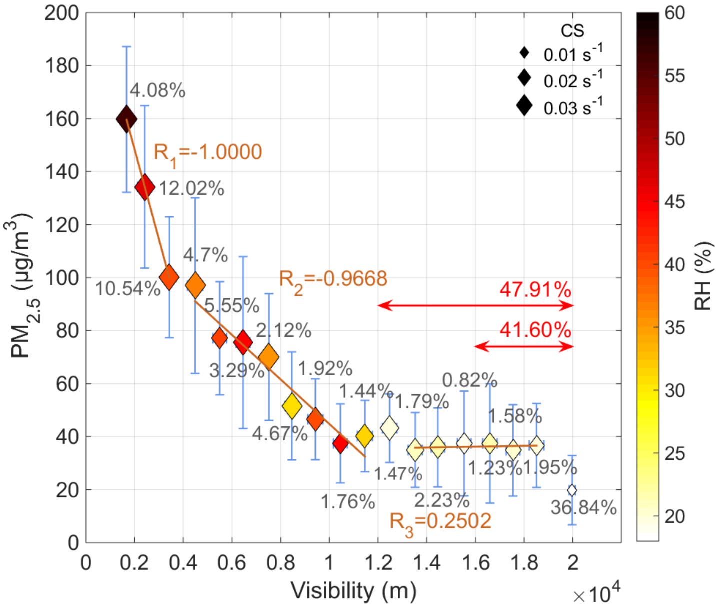

Fig. S3 Correlation between $PM_{2.5}$ and visibility during nighttime (20:00-04:00) from 18th January to 16th March 2019. The size is proportional to CS and the color is based on RH. Note that the data points are based on data averaged and binned into different visibility ranges instead of the original, high time resolution data. The error bars are the standard deviation of all data points in each bin.

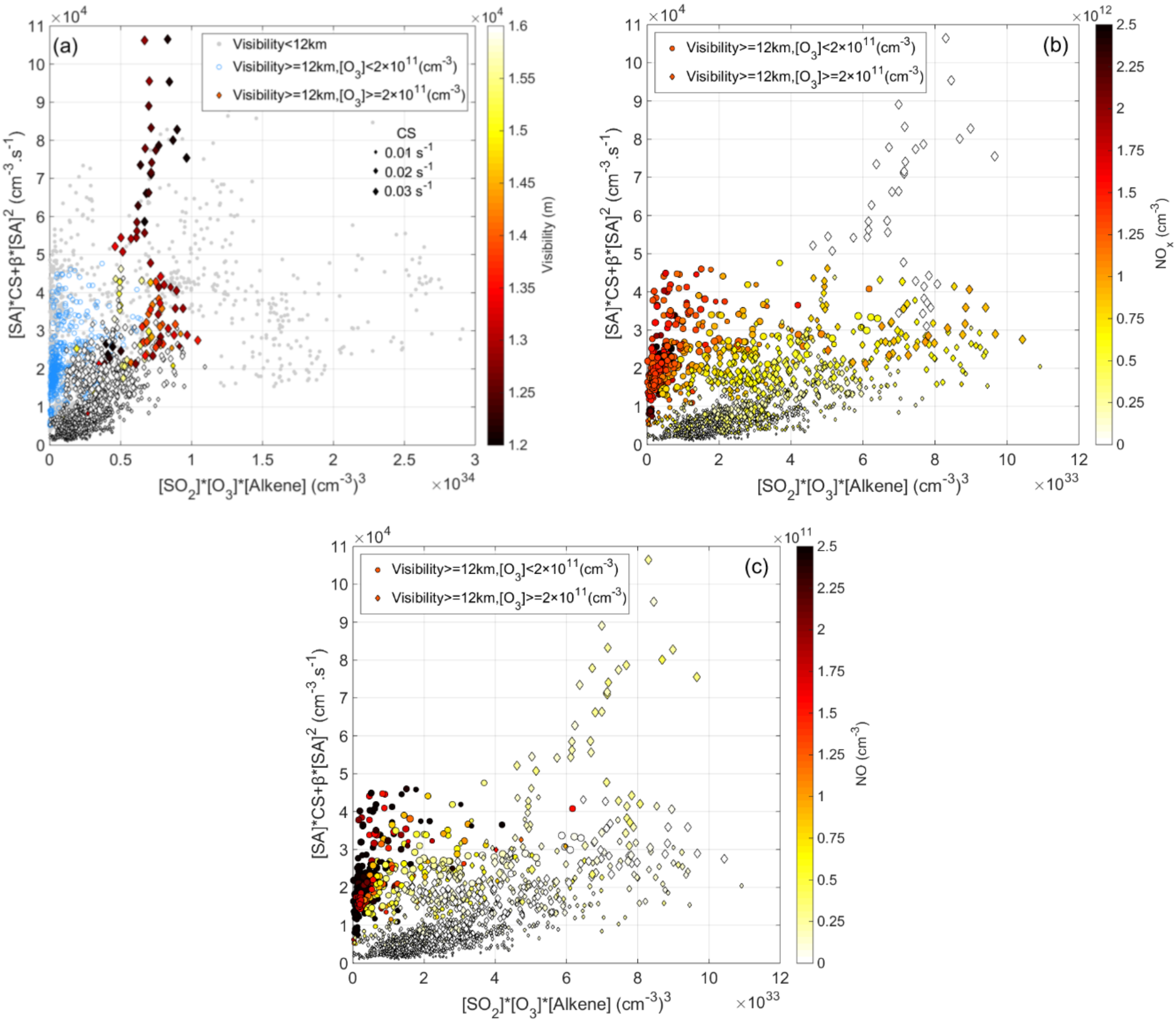

Fig. S4 Nighttime correlation between the source term ($[SO_2]\cdot[O_3]\cdot[Alkene]$) and sink term ($[SA]\cdot CS+\beta\cdot[SA]^2$) of SA under PSS assumption during nighttime (20:00-04:00) from 18th January to 16th March 2019 for (a) with all data points divided by O_3 concentration and visibility, (b) and (c) with data points having visibility larger than 12.0 km divided by $[O_3]$ and colored by NO_x and NO respectively.

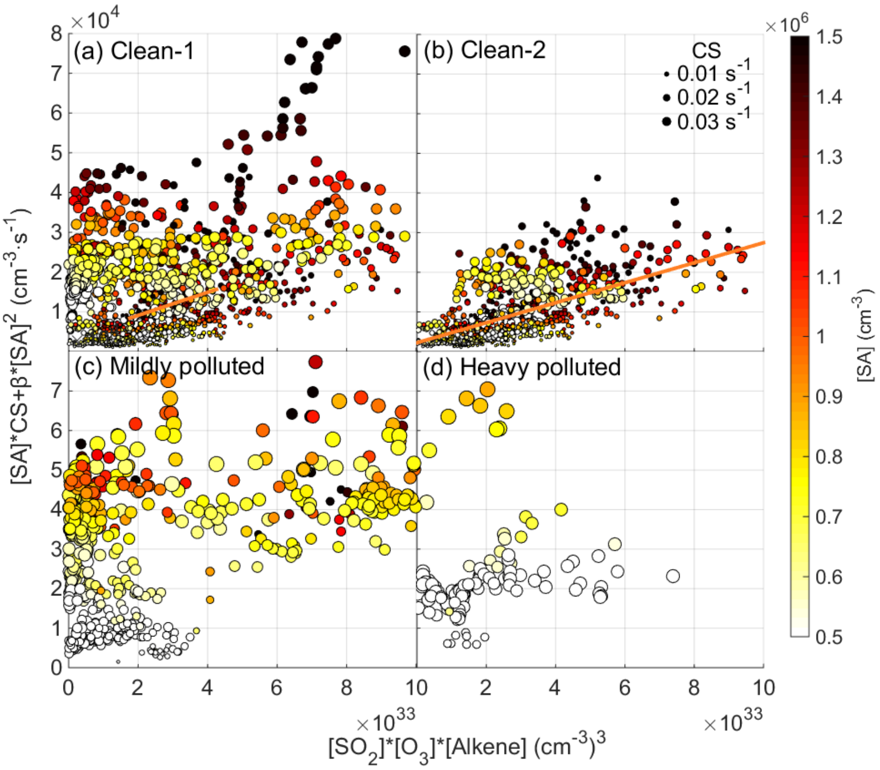

Fig. S5 Nighttime correlation between the source term ([SO_2]·[O_3]·[Alkene]) and sink term ([SA]·CS+β·[SA]^2) of SA under PSS assumption for (a) Clean-1 condition, (b) Clean-2 condition, (c) mildly polluted condition and (d) heavy polluted condition.

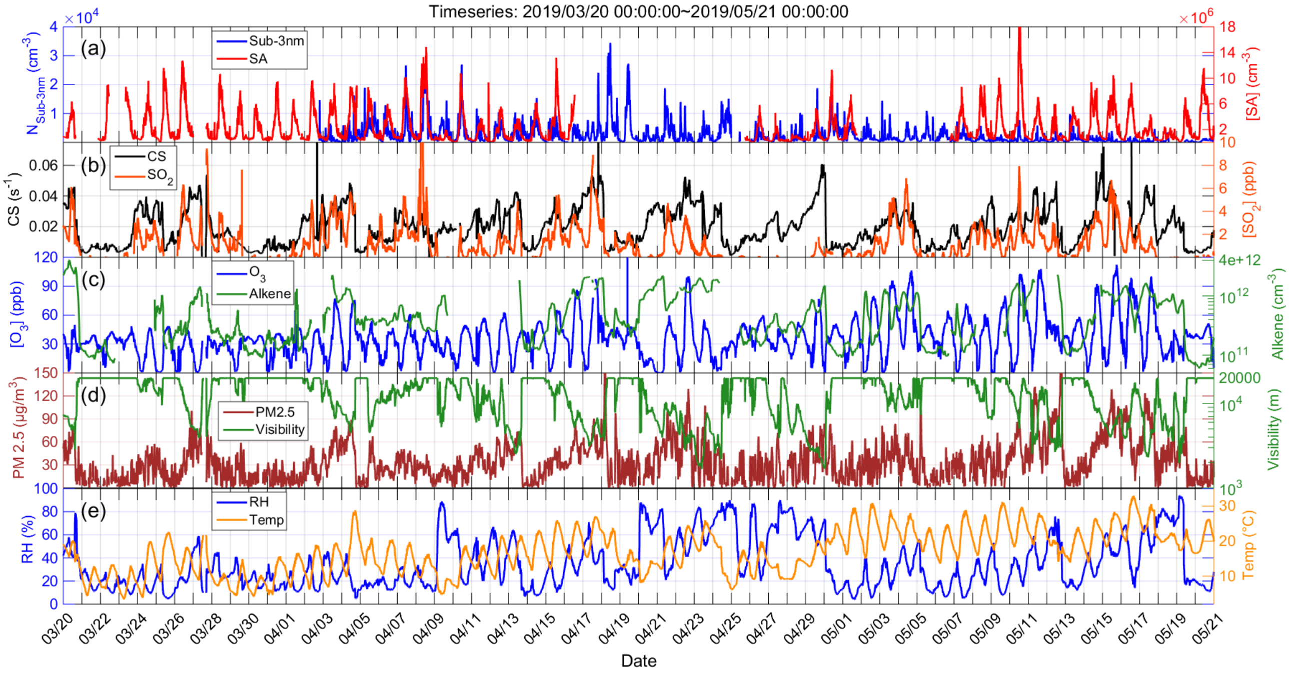

Fig. S6 Time variation of different parameters measured from 20th March to 20th May 2019 for (a) SA concentration and $N_{Sub\text{-}3nm}$, (b) CS and SO_2 concentration, (c) concentration of O_3 and alkenes, (d) $PM_{2.5}$ and visibility, and (e) relative humidity (RH) and temperature.

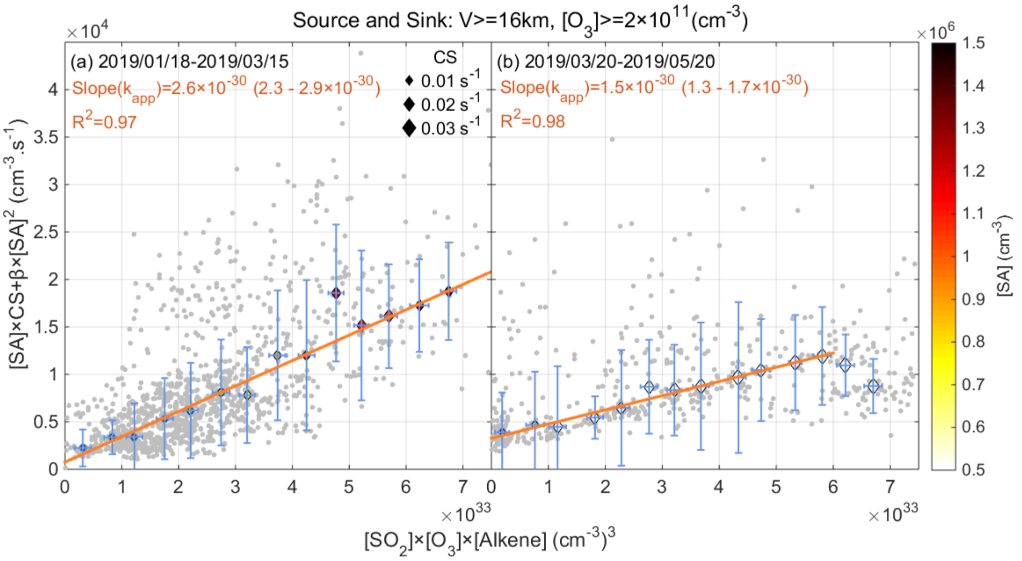

Fig. S7 Nighttime correlation between the source term ($[SO_2]\cdot[O_3]\cdot[Alkene]$) and sink term ($[SA]\cdot CS+\beta\cdot[SA]^2$) under clean conditions for (a) from 18th January to 16th March 2019 and (b) from 20th March to 20th May 2019. The gray dots are original, high time resolution data, and the diamond points are based on data median averaged and binned to different source ranges instead of the original, high time resolution data. The error bars are the standard deviation of all data points in each bin.

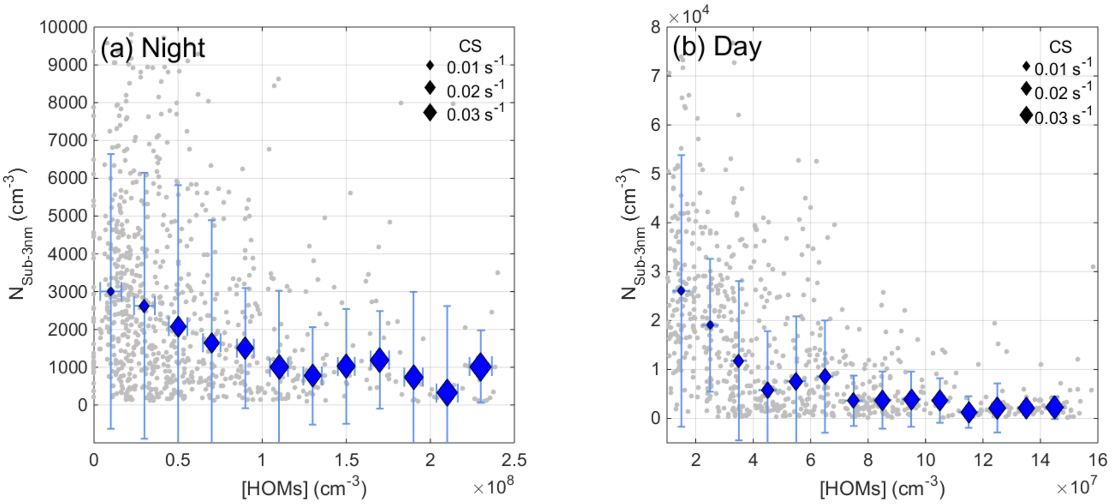

Fig. S8 Correlation between $N_{Sub\text{-}3nm}$ and number concentration of HOMs for (a) during nighttime (20:00-04:00) and (b) during daytime (09:00-16:00) from 18th January to 16th March 2019. Grey dots are original data, and diamonds are binned ones. The size of the binned data is proportional to CS and blue lines are standard deviation of each binned data.

Tables

Table S1 Dates of Nighttime SA event and non-event days.

Nighttime SA Event Day	Nighttime SA Non-event Day
2019.01.20	2019.01.24
2019.01.21	2019.01.30
2019.01.22	2019.02.03
2019.01.23	2019.02.06
2019.01.25	2019.02.08
2019.01.28	2019.02.11
2019.02.01	2019.02.13
2019.02.04	2019.02.21
2019.02.12	2019.02.22
2019.02.15	2019.02.27
2019.02.17	2019.03.04
2019.02.20	2019.03.06
2019.02.25	2019.03.07
2019.02.26	2019.03.09
2019.02.28	2019.03.10
2019.03.12	2019.03.11
2019.03.14	
2019.03.15	

Table S2 Features of Nighttime SA Event Cases on 18 Event Nights.

Date	Number of Nighttime SA Case	CS Decrease Case	SO_2 Increase Case	Other Cases
2019.01.20	1			1
2019.01.21	1	1		
2019.01.22	1	1		
2019.01.23	1	1		
2019.01.25	1	1		
2019.01.28	1			1
2019.02.01	1			1
2019.02.04	1		1	
2019.02.12	2	1	1	
2019.02.15	1	1		
2019.02.17	1		1	
2019.02.20	1	No CS data		
2019.02.25	1			
2019.02.26	2	2		
2019.02.28	1	No CS data		
2019.03.12	1	No CS data		
2019.03.14	1	No CS data		
2019.03.15	1	No CS data		
Total	15 with CS data (20 in total)	8 (53.33%*)	4 (26.67%*)	3 (20.00%*)

* There are 5 days when CS data is not available and the statistical percentages in the brackets are based on the CS available cases.

Table S3 Fitted value, 95% confidence bounds and uncertainty of k_{app} and R^2 for Clean-1 and Clean-2 condition.

Condition	k_{app} ($cm^6\ s^{-1}$)	95% Confidence Bounds ($cm^6\ s^{-1}$)	Uncertainty (%)	R^2
Clean-1	2.7×10^{-30}	(2.1×10^{-30} - 3.2×10^{-30})	20.2	0.97
Clean-2	2.6×10^{-30}	(2.3×10^{-30} - 2.9×10^{-30})	11.3	0.97

Table S4 Concentration, net concentration change, loss rate and production rate of SA during nighttime (20:00-04:00) from 18th January to 16th March 2019. Std means standard deviation.

	[SA] (cm^{-3})	d[SA]/dt ($cm^{-3}s^{-1}$)	L_{SA} ($cm^{-3}s^{-1}$)	P_{SA} ($cm^{-3}s^{-1}$)
Median	7.52×10^5	181.60	1.61×10^4	1.60×10^4
25 percentile	5.19×10^5	78.37	4.83×10^3	4.80×10^3
75 percentile	1.05×10^6	371.14	3.27×10^4	3.26×10^4

References

Jayne, J. T., Pöschl, U., Chen, Y.-m., Dai, D., Molina, L. T., Worsnop, D. R., Kolb, C. E., and Molina, M. J.: Pressure and Temperature Dependence of the Gas-Phase Reaction of SO_3 with H_2O and the Heterogeneous Reaction of SO_3 with H_2O/H_2SO_4 Surfaces, The Journal of Physical Chemistry A, 101, 10000-10011, 10.1021/jp972549z, 1997.